Title:

Circadian benefits of exercise training reflect metabolic and structural flexibility

Authors:

Drew Duglan[1], Nuria Casanova-Vallve[1], Megan E. Vaughan[1], Michal K. Handzlik[2], Weiwei Fan[3], Ruth T. Yu[3], Christopher Liddle[4], Michael Downes[3], Alanna B. Chan[1], Marie Pariollaud[1], Megan E. Afetian[1], Christian M. Metallo[2], Ronald M. Evans[3], and Katja A. Lamia[1,*]

Affiliations:

[1] Department of Molecular Medicine, Scripps Research, La Jolla, California 92037, USA.

[2] Department of Bioengineering, University of California, San Diego, La Jolla, CA 92093, USA.

[3] Gene Expression Laboratory, Salk Institute for Biological Studies, La Jolla, California 92037, USA.

[4] Storr Liver Centre, Westmead Institute for Medical Research and University of Sydney School of Medicine, Westmead Hospital, Westmead, NSW 2145, Australia.

*Correspondence to: klamia@scripps.edu

Abstract:

Identifying molecular adaptations underlying improved fitness in response to training is of critical interest in exercise physiology. Circadian rhythms broadly modulate metabolism, including muscle substrate utilization and exercise capacity. Here we show that time of day influences the increase in exercise capacity afforded by training: when maximum running speed is measured at the beginning of the nighttime active period in mice, there is no measurable benefit from training, while maximum increase in performance occurs at the end of the night. Incidentally, we describe an improved method to motivate running in rodent exercise studies that obviates the use of electrical stimulation. Furthermore, we describe daily rhythms in carbohydrate and lipid metabolism and transport associated with the time-dependent response to training. Thus, we show that circadian rhythms modulate muscle-intrinsic responses to training and provide resources for the optimal design of exercise studies in rodents.

Exercise performance can be modulated by diet, metabolism, and environmental factors including the time of day [1]. In athletes, physical performance is enhanced in the evening compared to the same exercise in the morning [2-5]. Similarly, sedentary mice exhibit improved endurance capacity late in the active period [6]. Thus, in both humans and rodents, time of day influences maximum exercise capacity with a similar relationship to circadian phase. However, the molecular underpinnings for this apparently conserved phenomenon are unknown.

Chronotype is a measure of a person's natural preference for sleep-wake timing and categorizes individuals as "night owls", "morning larks", or somewhere in between [7,8]. People with different chronotypes respond differently to the same exercise at the same time of the day [9]. This suggests that the unique internal clock in each subject can influence exercise performance and response to training. Furthermore, it has recently become clear that the time at which exercise is performed influences its impacts on physiology. Exercise adjusts circadian clock time, thus influencing sleep-wake timing; the degree and direction of the adjustment depends on the time at which exercise occurs as well as on chronotype [10,11]. Notably, the time of day at which exercise is performed seems to alter its beneficial impact in diabetic patients [12]. Taken together, these findings further support the hypothesis that exercise physiology and circadian rhythms are intimately intertwined and motivate our search for a deeper understanding of how they are connected at the molecular level.

The circadian clock is based on a transcriptional feedback loops [13] In which brain and muscle ARNT-like protein 1 (BMAL1) and circadian locomotor output cycles kaput (CLOCK) regulate thousands of target genes including their repressors encoded by the period (*Per1*, *Per2,* and *Per3*) and cryptochrome (*Cry1* and *Cry2*) genes. Circadian clocks dictate the rhythmic expression of metabolic target genes in anticipation of predictable daily fluctuations in demand. In skeletal muscle, genes involved in carbohydrate and lipid metabolism are enriched among those that exhibit rhythmic expression and those that are regulated by BMAL1 [14,15]. Consistent with these findings, the metabolic state of muscles and their response to acute exercise depends on time of

day [16,17]. Moreover, deletion of *Bmal1* results in impaired glucose metabolism [18,19], reduced grip strength, and increased muscle fibrosis [20]. Deletion of the circadian repressors *Cry1* and *Cry2* results in enhanced exercise performance and metabolic regulation with increased fatty acid oxidation, involving activation of PPARδ [21]. Finally, MYOD1, an important regulator of muscle cell differentiation was recently found to interact with BMAL1:CLOCK and to regulate downstream genes in a circadian manner in skeletal muscle [22].

The potential for circadian rhythms to influence exercise outcomes has long been recognized both in real-world and laboratory settings; time of day was included among the parameters to be considered in the design of exercise experiments involving animals by an expert panel of the American Physiological Society as early as 2006 [23]. That monograph also included a discussion of the use of “aversive stimuli” to motivate laboratory animals to exercise. The authors’ urged careful consideration of the use of mild electric shocks to motivate animals to run, mostly due to ethical considerations. Although electrical stimulation via the neuromuscular junction is well established to be a key physiological stimulant of muscle contraction, and electrical stimulation of muscle fibers *in vitro* is widely used to study physiological responses [24-26], surprisingly little research has addressed the potential confounding effect of the use of mild electrical stimulation in rodent exercise testing.

Here, we demonstrate that the impact of low intensity training on maximum sprint speed depends on the time of day. Notably, we find that the widespread use of electrical

stimulation to motivate running in rodent exercise testing dramatically alters experimental outcomes. We provide a comprehensive characterization of circadian transcriptome remodeling in response to training that reveals specific alterations in carbohydrate and lipid metabolism that support time of day differences in sprint exercise capacity in trained animals. We show that glycogen and lipid metabolism are key nodes connecting circadian rhythms and exercise physiology and establish resources that will enable further investigation of the molecular mechanisms underlying circadian rhythms in optimal exercise performance.

Results:

Electrical stimulation can alter outcomes in rodent treadmill tests

Given the significant impact of genetically deleting both of the circadian repressors *Cry1* and *Cry2* on sprint exercise capacity in mice [21], we hypothesized that maximum sprint exercise capacity may depend on the time of day. While others have reported that sedentary male mice exhibit enhanced sprint exercise capacity early in the night when CRY1/2 protein expression is lower [6], we found that time of day had no impact on maximum sprint speed in sedentary c57BL/6J male mice (Figs. 1A-B, S1A), despite using essentially the same time points, the same strain of mice, and the same sprint exercise testing protocol. Notably, the maximum speeds reported were much slower than the speeds that we measured. The only major difference in the testing protocols is the aversive stimulus used to motivate mice to continue running. We abandoned the common practice of using aversive electrical stimulation several years ago in favor of using gentler physical stimuli to motivate continued running because we suspected that

even mild electric shocks may influence outcomes [21]. In an effort to understand the remarkably slower maximum speeds reported by others, we compared maximum sprint speeds measured when continued running was motivated by either mild electrical stimulation or by our manual method (Figure 1C). Indeed, the use of electrical stimulation in exercise testing profoundly impairs outcomes (Figure 1D and Figure S1B).

Running wheel (RW) training increases maximum speed at ZT21 but not at ZT13 in male mice

Given the importance of metabolism for driving peripheral circadian rhythms as exemplified by the role of feeding time in setting the timing of peripheral clocks [27], we hypothesized that daily exercise would enhance muscle circadian rhythms, and may reveal an impact of time of day on maximum sprint exercise capacity. After six weeks of voluntary training by running wheel access, the enhanced speed afforded by that training is significantly greater during the nighttime active period (Figure 1B and Figure S1A). Surprisingly, there is no measurable increase in maximum sprint speed after six weeks of low intensity training when sprint testing is performed at ZT13. The increased sprint capacity after voluntary training when measured at ZT6 (Figure S1A) is similar to what we have measured in the past at ZT8 [21], demonstrating the consistency of our measurements across several years and when the assay is performed by different individual investigators. Importantly, the increased sprint capacity is due to voluntary running wheel training rather than age as male mice maintained in a cage without running wheel access did not improve their performance (Figure S1C). As expected, mice with access to running wheels gain less weight than sedentary counterparts

(Figure S1D). Notably, the temporal pattern of voluntary running wheel activity does not match the temporal pattern of maximum sprint capacity, as voluntary running at ZT13 is greater than at ZT21 (Figure 1E), while maximum trained speed is greater at ZT21. Finally, the impact of time of day on maximum sprint exercise capacity after six weeks of voluntary training was only observed in male mice. Female mice tend to be more active than males when provided running wheels (Figures S1E and S1F). Trained female mice have greater maximum sprint speed than their male counterparts, which was not different between ZT13 and ZT21 (Figure S1G).

RW training only mildly impacts core clock genes and Hif1a in skeletal muscle

To determine whether increased daily voluntary activity altered circadian rhythms of gene expression in muscles, we first used quantitative reverse transcriptase PCR (qPCR) to measure the basal expression of key circadian transcripts in quadriceps muscles from mice housed with or without running wheels for six weeks. This analysis revealed that enhanced daily activity increases the daily amplitude of *Per2* expression but did not generally enhance the amplitude of core clock genes (Figure 1F). While the profile of the PPARδ target gene *Pdk4* recapitulated our earlier finding of increased expression early in the day [21], it was not altered in response to training; nor was expression of the PPARδ coactivator *Ppargc1a* impacted. Together, these results suggest that basal activation of PPARδ does not play a major role in the response to low intensity training afforded by voluntary running wheel access, although chronic activation of PPARδ in muscles is well established to enhance exercise capacity [28-30],

and PPARδ is more robustly activated by acute intense exercise in trained mice than in sedentary controls [21].

Recently, several studies have demonstrated a close relationship between hypoxia signaling and circadian clocks, including suppression of HIF1α accumulation by the circadian repressors CRY1 and CRY2 [31,32], HIF1α control of circadian clock gene expression [33,34], and circadian modulation of *Hif1α* expression and of the transcriptional response to hypoxia [35,36]. In quadriceps of sedentary mice, *Hif1α* mRNA was elevated early in the day compared to other time points (Figure 1F). Training leads to a reduced transcriptional response to hypoxia [37]. Similar to the core circadian transcripts, *Hif1α* was only slightly altered by training: its expression was reduced at ZT1, resulting in loss of rhythmic expression. This seems unlikely to play a major role in the loss of response to hypoxia in trained muscles.

Increased expression of *Ldhb* has previously been recognized as a signature of the molecular response to low intensity training, and is believed to contribute to increased endurance exercise performance by enhancing the ability to utilize lactate as a fuel source [38,39]. We measured robustly enhanced expression of *Ldhb* after chronic low intensity exercise training (Figure 1F). There was no impact of time of day on *Ldhb* expression in sedentary or trained mice. In sedentary animals, we measured greater *Ldha* expression in quadriceps during the late night and the reduction of its expression after training was greater at ZT17 than at other times measured.

Il-6 expression in muscles and circulating levels of IL-6 increase rapidly in response to intense exercise [40]. Although circulating levels of IL-6 have been reported to change in response to regular exercise in humans, the impact of training on IL-6 production remains unclear [41]. Unlike *Ldhb*, we did not measure any increase in *Il-6* expression after six weeks of voluntary running wheel training. Induction of *Il-6* is correlated with glycogen depletion. Low intensity voluntary training may not affect muscle glycogen content enough to increase *Il-6* expression relative to sedentary mice. Regardless, changes in *Il-6* expression within muscles do not seem to be required for the training-induced enhancement of sprint exercise capacity at ZT21 in this study. However, as reported in macrophages [42], we observed a robust daily oscillation of *Il-6* expression in quadriceps muscles regardless of training state (Figure 1F).

RW training dramatically remodels the muscle circadian transcriptome

Because circadian clocks are best characterized as transcription-translation feedback loops and to take advantage of the rich literature on circadian regulation of transcription, we used high throughput RNA sequencing to measure the impact of daily voluntary wheel running on circadian mRNA expression patterns. For this experiment, we established a new group of male c57BL/6J mice that were transferred to singly housed cages at the age of 9 weeks. Half were provided access to running wheels (trained) and half were not (sedentary). Six weeks later, we collected plantaris muscles every four hours from each group over a 24-hour period (Figure 2A) for RNA sequencing to get a better sense of the impact of low intensity exercise training on circadian gene expression globally. Note that plantaris and quadriceps muscles are expected to have

similar global patterns of gene expression [43]. Principal component analysis provided confidence in the quality of our samples: samples clustered by circadian time and training state (Figure 2B).

We used several complementary approaches to analyze genome-wide expression patterns. Using CircWave [44], we identified transcripts with temporal profiles consistent with rhythmic expression in plantaris muscles from sedentary or trained male mice with a false discovery rate of five percent (pANOVA < 0.05). This analysis supports the hypothesis that daily rhythmic voluntary running increases daily rhythms of gene expression within muscles (Figs. 2C, 2D). However, as in quadriceps, this does not seem to reflect global increased amplitude of core clock gene expression in plantaris (Fig 2E). Although their rhythmic mRNA profiles exhibit a phase difference of ~8 hours (Figure 2E), we found that CRY1 and CRY2 protein rhythms in plantaris muscles are synchronous, peaking late in the dark phase (Figure 2F). Intriguingly, CRY1 is elevated in the muscles of mice housed with access to a running wheel across all times of day and night (Figures 2F and 2G).

We used differential expression analysis to identify the transcripts most impacted by the enhanced activity afforded by access to a running wheel (with zeitgeber time as a confounding factor) (Figure 3A). Among the 50 transcripts that are most up- or down-regulated in trained mice compared to sedentary mice, we identified several well-established training-responsive transcripts. For example, calsequestrin 2 (*Casq2*) promotes calcium storage in sarcoplasmic reticulum of slow oxidative muscles and its

expression is enhanced in our trained mice (Figure 3A and Figure S2). Myosin heavy chain isoform expression also changed as expected in response to low intensity exercise training: the genes encoding myosin heavy chains 2 and 4 (*Myh2* and *Myh4*) were among the top increased and decreased transcripts, respectively (Figure 3B). This indicates that plantaris muscles contain a greater proportion of Type IIa fibers and reduced type IIb fibers after six weeks of voluntary running. This is consistent with the low intensity and long duration of the voluntary running activity that occurs with providing access to a running wheel, which is expected to enhance the proportion of oxidative fiber types within mixed muscle groups like the plantaris, and is expected to increase endurance exercise capacity. We extracted expression data from other myosin heavy chain isoforms that are commonly used to measure fiber types. Surprisingly, the expression of the type I fiber marker *Myh7* is highly impacted by the time of day in plantaris muscles of sedentary animals, suggesting that the time of sample collection may impact quantitation of muscle fiber types using qPCR in sedentary mice. It is unclear whether this dramatic daytime-dependent expression of *Myh7* mRNA (Figure 3B) has any functional importance given the long half-life of myosin heavy chain proteins.

As in quadriceps, *Ldhb* expression was consistently enhanced by activity in plantaris muscles (Figures 3A and 3C), supporting the idea that our protocol reproduces established signatures of enhanced endurance exercise capacity in response to training. *Ldha* expression was reduced in plantaris muscle of trained mice and was not significantly altered by zeitgeber time. Together, these results suggest that lactate

dehydrogenase isozyme expression is unlikely to contribute to the impact of time of day that we observed in sprint exercise capacity in trained mice.

In addition to the observed changes in myosin heavy chain expression and *Ldhb*, we found that transcripts encoding structural components of muscles and metabolic enzymes are overrepresented among those most responsive to increased daily activity. Intriguingly, several of these exhibit striking daytime-dependent expression, which may explain why their regulation by exercise state has not been observed previously (Figure 3D and Figure S2). For example, the transcript encoding diacylglycerol O-acyltransferase 2 (DGAT2, an enzyme that catalyzes the final step in the synthesis of triglycerides) is slightly elevated in trained muscles during the day and its expression is six-fold higher in trained muscles compared to sedentary at ZT13 (Figure 3D). Furthermore, DGAT2 protein exhibits dramatically increased accumulation in plantaris muscles of trained mice only during the night, with peak abundance measured at ZT13-ZT17 (Figure 3E).

Similar to *Dgat2*, expression of the estrogen-related receptors beta (*Esrrb*) and gamma (*Esrrg*) was not dependent on time of day in muscles from sedentary mice, consistent with prior studies of circadian regulation of nuclear hormone receptor expression in metabolic tissues [45]. However, their expression became dramatically dependent on time of day in plantaris muscles of trained mice (Figure 3D and Figure S2). Notably, *Esrrg* expression is high in oxidative muscle fibers, and transgenic expression of *Esrrg* enhances oxidative metabolism and angiogenesis in muscles that do not normally

express it [46] so its increased expression in response to daily activity likely contributes to metabolic and vascular remodeling. This has not been previously reported, and demonstrates the value of considering time of day in experimental design.

Even more surprising than the circadian regulation of metabolic enzymes that are increased in response to elevated daily activity is that we observed strong time of day effects on the expression of several transcripts that encode components of muscle cytoskeletal and sarcomere structures (Figure 3D and Figure S2). Although rhythmic gene expression does not always translate to rhythmic protein abundance, we measured time of day dependent accumulation of the actin filament anchoring protein crystallin alpha B (CRYAB) in trained plantaris muscles (Figure 3E), suggesting that muscle structural features undergo daily remodeling.

Voluntary RW training and time of day coordinately influence glycogen metabolism

We used gene set enrichment analysis (GSEA)[47,48] to identify pathways defined in MSigDB [49,50] that are significantly impacted by training. Transcripts involved in glycogen metabolism were highly enriched among those altered by training (Figure 4A-B). Specifically, the expression of several enzymes involved in glycogen breakdown is reduced in plantaris muscles of trained compared to sedentary male mice (Figure 4C). In addition, the expression of several enzymes and regulatory factors that contribute to glycogen synthesis depends on the time of day (Figure 4D). Glycogen synthase kinases 3 alpha (GSK3α) and beta (GSK3β) phosphorylate glycogen synthase and inhibit its

activity. At the protein level, we measured a tendency for GSK3α and GSK3β to be reduced at ZT21 compared to ZT13 in quadriceps of trained mice (Figures 4E, 4F and Figure S3A). Hexokinase 2 (HK2) phosphorylates glucose to produce glucose-6-phosphate, which is required for entry into glycogen synthesis or glycolysis. Not only was *Hk2* transcript expressed rhythmically, HK2 protein was significantly lower in quadriceps muscles of trained mice at ZT21 compared to those collected at ZT13 (Figures 4E and 4G).

Intramuscular glycogen provides fuel for energy production during intense exercise. The apparent regulation of glycogen synthesis and breakdown by both training and time of day suggests that this could play an important role in the observed impact of time of day on maximum sprint speed in trained mice. Indeed, quadriceps muscles of trained male mice contain three times more glycogen at ZT21 than they do at ZT13 (Figure 4H and Figure S3B). In addition, male mice seem to break down glycogen more slowly during a sprint exercise test performed at ZT21 than at ZT13 (Figure 4I). Together, these findings suggest that altered glycogen metabolism is an important component of increased maximum running speed at the end of the active period in trained mice. Further supporting this idea, we measured a significant correlation between quadriceps glycogen depletion and treadmill failure in trained mice (Figure 4J). Liver glycogen content was higher at ZT21 regardless of training state, and its depletion was less well correlated with treadmill failure (Figs. 4K-M). Similar to their greater maximum sprint speed, the glycogen content of female quadriceps muscles was greater than that of males and while it also tended to be greater at ZT21 than at ZT13, the difference was

not statistically significant (Figure S3C); liver glycogen content tended to be lower in female mice and also tended to be greater at ZT21 than at ZT13 regardless of sedentary or trained status (Figure S3D).

Training impacts carbohydrate and lipid metabolism in a time of day dependent manner

We ranked all detected transcripts by the statistical evaluation of rhythmicity from CircWave (pANOVA) and used this pre-ranked list to search for gene sets enriched in rhythmic expression in plantaris from either sedentary or trained mice. Transcripts involved in oxidative phosphorylation are overrepresented among genes that exhibit rhythmic expression patterns in sedentary animals but not in animals trained via voluntary wheel access (Figure 5A). Querying gene ontology [51] gene sets using GSEA revealed that transcripts encoding sodium symporters are enriched among those with greater rhythmicity in the trained state (Figure 5B). Of particular interest for exercise physiology, transporters that enable the import of the high energy metabolites creatine (SLC6A8), phosphate (SLC20A1) and taurine (SLC6A6) exhibit elevated expression specifically late in the nighttime active period in trained plantaris muscles (Figures 5B and 5C).

The significantly altered expression of transcripts and protein complexes involved in oxidative phosphorylation, and strong nighttime expression of DGAT2, suggest that enhanced storage and utilization of lipids as fuel sources late in the active period of trained male mice could allow them to conserve intramuscular glycogen. We used

targeted metabolomic profiling to measure the content of twenty-five fatty acid species with varying chain lengths and saturation. While the total triacylglyceride (TAG) content of quadriceps muscles was affected neither by time of day nor by prior training (Figure 5D), the acyl chain content of intramuscular lipids was remodeled by time of day and level of daily activity. Several long-chain TAGs, specifically those containing 18:2 carbohydrate chains, were increased in quadriceps of trained male mice collected at ZT21 but not at ZT13 (Figure 5E and Figure S4A), while TAG species with shorter fatty acid tails were reduced. This finding supports the hypothesis that trained male mice subjected to sprint exercise testing at ZT21 are able to conserve muscle glycogen stores by burning alternative fuel sources, which in turn likely facilitates greater maximum running speed. The observed changes in lipid fatty acyl chain content suggests altered activity of lipid chain remodeling enzymes. Indeed, *Elovl1* and *Elovl5*, the only elongases detected above the threshold of 1 FPKM, exhibit elevated expression in trained muscles, particularly late in the active period (Figure 5F).

The major sources of energy production in exercising muscles are amino acids, carbohydrates, and lipids. We used targeted metabolite profiling to measure these broad categories in quadriceps muscles of sedentary and trained mice at ZT13 and ZT21. Neither time of day nor activity level was associated with major changes in amino acid content (Figure S4B). However, both carbohydrate and lipid profiles were significantly altered by exercise training in a time of day dependent manner. Glycolytic intermediates tended to be elevated at ZT21 compared to ZT13 in sedentary mice, and fumarate and malate were significantly increased in trained mice compared to sedentary

mice at ZT13, but not at ZT21 (Figure S4C). Further supporting the hypothesis that trained male mice generate a greater proportion of the energy required to fuel sprint exercise by burning fatty acids at ZT21 than they do at ZT13, they have reduced circulating non-esterified fatty acids (NEFA) (Figure 5G) and glycerol (Figure 5H) after sprinting to exhaustion at ZT21 compared to those exercised at ZT13. Furthermore, they maintain stable levels of glucose and beta hydroxybutyrate in circulation after the sprint test, while trained mice at ZT13 experience a significant reduction of blood glucose (Figure 5I) and an increase in circulating ketone bodies (Figure 5J). Blood lactate increased after exercise with a greater elevation at ZT21 (Figure 5K).

Discussion:

In contrast to a recent report [6], we did not observe any difference in sprint exercise capacity of sedentary male c57BL/6J when it was measured at ZT13 and ZT21. While research has not previously addressed the potential confounding impact of the use of electrical stimulation as an aversive stimulus to motivate treadmill running in rodents, another recent study used a manual method similar to the one that we employed to avoid the use of electrical stimulation in research using animals treated with chemotherapy [52]. Notably, they report similar maximum speeds in control animals as those we observe in sedentary mice, further supporting the reproducibility of findings using this manual method. Further investigation will be required to understand the mechanistic basis for the much earlier termination of sprint exercise testing when an aversive electrical stimulus is used to motivate continued running. However, so-called freezing behavior in response to mild electric shocks has long been used as a readout

in fear conditioning experiments [53], and this behavioral response may contribute to what appears to be a failure to continue running. Regardless, it is important to recognize that electrical stimulation confounds exercise outcomes given the widespread use of this method to motivate continued treadmill running in exercise research using rodents.

In contrast to our finding that maximum sprint speed is indistinguishable between ZT13 and ZT21 in sedentary animals, male mice robustly increased their maximum sprint capacity in a striking time of day dependent manner after six weeks of running wheel training. As we [32] and others [54] have seen in prior studies, female mice tend to be more active than males; in addition, both maximum speed and tissue glycogen content are significantly greater in trained c57BL/6J female mice than they are in males. The explanation for this robust sexual dimorphism is unclear [54]. Nevertheless, the effect of time of day on the beneficial impact of low intensity training on maximum sprint speed in male mice enables us to elucidate which molecular changes in response to training are sufficient and/or required for enhanced sprint exercise capacity. Many established molecular responses to low intensity training [55] were equivalent at ZT13 and ZT21 while maximum speed was increased only at ZT21. Molecular differences between the sedentary and trained mice across the circadian cycle indicates that circadian remodeling of carbohydrate and lipid metabolism and transport within skeletal muscles underlie the observed time-dependent enhancement in performance.

We measured a dramatic remodeling of the daily rhythms of gene expression in plantaris muscles in response to six weeks of voluntary running wheel training. In

general, a greater proportion of the genome exhibits daily rhythms of gene expression in trained mice, consistent with a prior report that muscle groups containing a greater proportion of oxidative fibers exhibit more rhythmic transcription [56]. Among the most striking examples of a transcript activated by training specifically during the nighttime active phase is that encoding an enzyme that catalyzes a rate-limiting step in lipid biosynthesis, DGAT2. We confirmed that DGAT2 protein abundance is dramatically increased in the late active phase and this, combined with elevated expression of elongating enzymes (e.g. *Elovl1*, *Elovl5*), likely influences the greater accumulation of long chain lipids measured in quadriceps muscles isolated at that time. Previous studies have established the BMAL1-associated complement of mouse liver [57] and muscle [14] chromatin. In both cases, *Dgat2, Elovl1,* and *Elovl5* were found to be targeted by BMAL1 at multiple sites. Thus, BMAL1 directly activates these lipid synthesizing enzymes and this likely enables the strong circadian regulation of their enhanced expression in response to exercise training. Furthermore, genes involved in carbohydrate and lipid metabolism were enriched among those altered by genetic deletion of BMAL1 in muscle [18]. However, not all BMAL1 targets were so clearly altered by training in a time of day dependent manner. While we saw an increase in rhythmic gene expression overall, many core clock transcripts unexpectedly did not exhibit enhanced circadian amplitude in trained mice (Figs. 1F and 2E). Because mice in the trained group continually had access to running wheels including on the day of sacrifice, it is unclear whether the observed patterns of gene expression reflect an acute response to voluntary running or a true remodeling of circadian expression in the absence of the recurring external stimulus.

The modulation of lipid metabolism in response to training is of particular interest in light of the so-called “athletes’ paradox” recognizing that intra-myocellular lipids are elevated in endurance trained athletes to levels similar to those observed in diabetic patients [58], while athletes’ insulin sensitivity remains robust. Coordinated elevation of lipid storage and oxidation in trained muscles likely explains the lack of pathological consequences [59]. Circadian modulation of these pathways may enable temporal coordination of lipid storage and utilization in the trained state to optimize performance while preventing detrimental impacts on overall metabolic health. While we did not observe an impact of time of day on total muscle TAG content, more detailed analyses would be required to measure intra-myocellular lipid content and to determine whether it is under circadian control.

Additional investigation will be required to understand how circadian clocks interact with exercise training of various types to coordinate changes in gene expression and physiology that ultimately determine exercise capacity. Understanding the relationship between chronobiology and exercise physiology will benefit athletic and military professionals to find the best time of the day for training and performance. Furthermore, incorporating principles of chronobiology into training regimens could provide a safer and more effective alternative to supplements and doping for improving physical performance. More broadly, exercise is among the most effective strategies for the prevention and treatment of metabolic disease. Indeed, increased exercise capacity is among the best correlates of overall health as indicated by reduced all-cause mortality

[60]. Improved understanding of how time of day influences the benefits of exercise training will improve its application in public health.

ACKNOWLEDGMENTS

This work was funded by NIH grants R01 DK112927 (to K.A.L. and C.M.M.), R01CA234245 (to C. M.M.), and DK057978 (to R.M.E.). R.M.E. is an investigator of the Howard Hughes Medical Institute at the Salk Institute and March of Dimes Chair in Molecular and Developmental Biology. We thank Simon Schenk, Sabine Jordan, Robert Farese, Tobias Walther, Julien Delezie, Geraldine Maier, and Christoph Handschin for helpful discussions, sharing of technical expertise, equipment, and reagents, and/or critical reading of the manuscript, and T. Thomas and Y. Slivers for administrative assistance.

AUTHOR CONTRIBUTIONS

D.D., N.C.V., M.V., M.K.H., W.F., A.B.C., M.P., M.A., and K.A.L. performed experiments; D.D., N.C.V., M.V., M.K.H., R.Y., C.L., M.D., C.M.M., and K.A.L. analyzed data; N.C.V. and K.A.L. made figures and wrote the paper with input from the other authors; R.M.E., C.M.M., and K.A.L. conceived and supervised the study. All authors edited and approved the manuscript.

COMPETING INTERESTS

Authors declare no competing interests.

REFERENCES:

1 Duglan, D. & Lamia, K. A. Clocking In, Working Out: Circadian Regulation of Exercise Physiology. *Trends in endocrinology and metabolism: TEM* **30**, 347-356, doi:10.1016/j.tem.2019.04.003 (2019).

2 Bessot, N. *et al.* The effect of pedal rate and time of day on the time to exhaustion from high-intensity exercise. *Chronobiology international* **23**, 1009-1024, doi:10.1080/07420520600920726 (2006).

3 Chtourou, H. & Souissi, N. The effect of training at a specific time of day: a review. *Journal of strength and conditioning research* **26**, 1984-2005, doi:10.1519/JSC.0b013e31825770a7 (2012).

4 Fernandes, A. L. *et al.* Effect of time of day on performance, hormonal and metabolic response during a 1000-M cycling time trial. *PloS one* **9**, e109954, doi:10.1371/journal.pone.0109954 (2014).

5 Lok, R., Zerbini, G., Gordijn, M. C. M., Beersma, D. G. M. & Hut, R. A. Gold, silver or bronze: circadian variation strongly affects performance in Olympic athletes. *Scientific reports* **10**, 16088, doi:10.1038/s41598-020-72573-8 (2020).

6 Ezagouri, S. *et al.* Physiological and Molecular Dissection of Daily Variance in Exercise Capacity. *Cell metabolism* **30**, 78-91 e74, doi:10.1016/j.cmet.2019.03.012 (2019).

7 Roenneberg, T., Wirz-Justice, A. & Merrow, M. Life between clocks: daily temporal patterns of human chronotypes. *Journal of biological rhythms* **18**, 80-90, doi:10.1177/0748730402239679 (2003).

8 Horne, J. A. & Ostberg, O. A self-assessment questionnaire to determine morningness-eveningness in human circadian rhythms. *International journal of chronobiology* **4**, 97-110 (1976).

9 Facer-Childs, E. & Brandstaetter, R. The impact of circadian phenotype and time since awakening on diurnal performance in athletes. *Current biology : CB* **25**, 518-522, doi:10.1016/j.cub.2014.12.036 (2015).

10 Youngstedt, S. D., Elliott, J. A. & Kripke, D. F. Human circadian phase-response curves for exercise. *The Journal of physiology*, doi:10.1113/JP276943 (2019).

11 Thomas, J. M. *et al.* Circadian rhythm phase shifts caused by timed exercise vary with chronotype. *JCI insight* **5**, doi:10.1172/jci.insight.134270 (2020).

12 Savikj, M. *et al.* Afternoon exercise is more efficacious than morning exercise at improving blood glucose levels in individuals with type 2 diabetes: a randomised crossover trial. *Diabetologia* **62**, 233-237, doi:10.1007/s00125-018-4767-z (2019).

13 Partch, C. L., Green, C. B. & Takahashi, J. S. Molecular architecture of the mammalian circadian clock. *Trends in cell biology* **24**, 90-99, doi:10.1016/j.tcb.2013.07.002 (2014).

14 Dyar, K. A. *et al.* Transcriptional programming of lipid and amino acid metabolism by the skeletal muscle circadian clock. *PLoS biology* **16**, e2005886, doi:10.1371/journal.pbio.2005886 (2018).

15 Hodge, B. A. *et al.* The endogenous molecular clock orchestrates the temporal separation of substrate metabolism in skeletal muscle. *Skeletal muscle* **5**, 17, doi:10.1186/s13395-015-0039-5 (2015).

16 Dyar, K. A. *et al.* Atlas of Circadian Metabolism Reveals System-wide Coordination and Communication between Clocks. *Cell* **174**, 1571-1585 e1511, doi:10.1016/j.cell.2018.08.042 (2018).

17 Sato, S. *et al.* Time of Exercise Specifies the Impact on Muscle Metabolic Pathways and Systemic Energy Homeostasis. *Cell metabolism* **30**, 92-110 e114, doi:10.1016/j.cmet.2019.03.013 (2019).

18 Harfmann, B. D. *et al.* Muscle-specific loss of Bmal1 leads to disrupted tissue glucose metabolism and systemic glucose homeostasis. *Skeletal muscle* **6**, 12, doi:10.1186/s13395-016-0082-x (2016).

19 Dyar, K. A. *et al.* Muscle insulin sensitivity and glucose metabolism are controlled by the intrinsic muscle clock. *Molecular metabolism* **3**, 29-41, doi:10.1016/j.molmet.2013.10.005 (2014).

20 Schroder, E. A. *et al.* Intrinsic muscle clock is necessary for musculoskeletal health. *The Journal of physiology* **593**, 5387-5404, doi:10.1113/JP271436 (2015).

21 Jordan, S. D. *et al.* CRY1/2 Selectively Repress PPARdelta and Limit Exercise Capacity. *Cell metabolism* **26**, 243-255 e246, doi:10.1016/j.cmet.2017.06.002 (2017).
22 Hodge, B. A. *et al.* MYOD1 functions as a clock amplifier as well as a critical co-factor for downstream circadian gene expression in muscle. *eLife* **8**, doi:10.7554/eLife.43017 (2019).
23 PROTOCOLS, A. P. S. C. T. D. A. A. R. B. F. T. D. O. A. E. *Resource Book for the Design of Animal Exercise Protocols*. (2006).
24 da Silva, L. P., Kundu, S. C., Reis, R. L. & Correlo, V. M. Electric Phenomenon: A Disregarded Tool in Tissue Engineering and Regenerative Medicine. *Trends in biotechnology* **38**, 24-49, doi:10.1016/j.tibtech.2019.07.002 (2020).
25 Hernandez-Ochoa, E. O. & Schneider, M. F. Voltage sensing mechanism in skeletal muscle excitation-contraction coupling: coming of age or midlife crisis? *Skeletal muscle* **8**, 22, doi:10.1186/s13395-018-0167-9 (2018).
26 Bannister, R. A. Bridging the myoplasmic gap II: more recent advances in skeletal muscle excitation-contraction coupling. *The Journal of experimental biology* **219**, 175-182, doi:10.1242/jeb.124123 (2016).
27 Damiola, F. *et al.* Restricted feeding uncouples circadian oscillators in peripheral tissues from the central pacemaker in the suprachiasmatic nucleus. *Genes & development* **14**, 2950-2961 (2000).
28 Narkar, V. A. *et al.* AMPK and PPARdelta agonists are exercise mimetics. *Cell* **134**, 405-415, doi:S0092-8674(08)00838-6 [pii]
10.1016/j.cell.2008.06.051 (2008).
29 Wang, Y. X. *et al.* Regulation of muscle fiber type and running endurance by PPARdelta. *PLoS biology* **2**, e294, doi:10.1371/journal.pbio.0020294 (2004).
30 Fan, W. *et al.* PPARdelta Promotes Running Endurance by Preserving Glucose. *Cell metabolism* **25**, 1186-1193 e1184, doi:10.1016/j.cmet.2017.04.006 (2017).
31 Dimova, E. Y. *et al.* The Circadian Clock Protein CRY1 Is a Negative Regulator of HIF-1alpha. *iScience* **13**, 284-304, doi:10.1016/j.isci.2019.02.027 (2019).
32 Vaughan, M. E. *et al.* Cryptochromes Suppress HIF1alpha in Muscles. *iScience* **23**, 101338, doi:10.1016/j.isci.2020.101338 (2020).
33 Adamovich, Y., Ladeuix, B., Golik, M., Koeners, M. P. & Asher, G. Rhythmic Oxygen Levels Reset Circadian Clocks through HIF1alpha. *Cell metabolism* **25**, 93-101, doi:10.1016/j.cmet.2016.09.014 (2017).
34 Peek, C. B. *et al.* Circadian Clock Interaction with HIF1alpha Mediates Oxygenic Metabolism and Anaerobic Glycolysis in Skeletal Muscle. *Cell metabolism* **25**, 86-92, doi:10.1016/j.cmet.2016.09.010 (2017).
35 Manella, G. *et al.* Hypoxia induces a time- and tissue-specific response that elicits intertissue circadian clock misalignment. *Proceedings of the National Academy of Sciences of the United States of America* **117**, 779-786, doi:10.1073/pnas.1914112117 (2020).
36 Wu, Y. *et al.* Reciprocal Regulation between the Circadian Clock and Hypoxia Signaling at the Genome Level in Mammals. *Cell metabolism* **25**, 73-85, doi:10.1016/j.cmet.2016.09.009 (2017).
37 Lindholm, M. E. *et al.* Negative regulation of HIF in skeletal muscle of elite endurance athletes: a tentative mechanism promoting oxidative metabolism.

American journal of physiology. Regulatory, integrative and comparative physiology **307**, R248-255, doi:10.1152/ajpregu.00036.2013 (2014).

38 Apple, F. S. & Rogers, M. A. Skeletal muscle lactate dehydrogenase isozyme alterations in men and women marathon runners. *Journal of applied physiology* **61**, 477-481, doi:10.1152/jappl.1986.61.2.477 (1986).

39 Liang, X. *et al.* Exercise Inducible Lactate Dehydrogenase B Regulates Mitochondrial Function in Skeletal Muscle. *The Journal of biological chemistry* **291**, 25306-25318, doi:10.1074/jbc.M116.749424 (2016).

40 Steensberg, A. *et al.* IL-6 and TNF-alpha expression in, and release from, contracting human skeletal muscle. *American journal of physiology. Endocrinology and metabolism* **283**, E1272-1278, doi:10.1152/ajpendo.00255.2002 (2002).

41 Gorgens, S. W., Eckardt, K., Jensen, J., Drevon, C. A. & Eckel, J. Exercise and Regulation of Adipokine and Myokine Production. *Progress in molecular biology and translational science* **135**, 313-336, doi:10.1016/bs.pmbts.2015.07.002 (2015).

42 Keller, M. *et al.* A circadian clock in macrophages controls inflammatory immune responses. *Proceedings of the National Academy of Sciences of the United States of America* **106**, 21407-21412, doi:0906361106 [pii] 10.1073/pnas.0906361106 (2009).

43 Terry, E. E. *et al.* Transcriptional profiling reveals extraordinary diversity among skeletal muscle tissues. *eLife* **7**, doi:10.7554/eLife.34613 (2018).

44 Oster, H., Damerow, S., Hut, R. A. & Eichele, G. Transcriptional profiling in the adrenal gland reveals circadian regulation of hormone biosynthesis genes and nucleosome assembly genes. *Journal of biological rhythms* **21**, 350-361, doi:10.1177/0748730406293053 (2006).

45 Yang, X., Lamia, K. A. & Evans, R. M. Nuclear receptors, metabolism, and the circadian clock. *Cold Spring Harbor symposia on quantitative biology* **72**, 387-394, doi:10.1101/sqb.2007.72.058 (2007).

46 Narkar, V. A. *et al.* Exercise and PGC-1alpha-independent synchronization of type I muscle metabolism and vasculature by ERRgamma. *Cell metabolism* **13**, 283-293, doi:10.1016/j.cmet.2011.01.019 (2011).

47 Subramanian, A. *et al.* Gene set enrichment analysis: a knowledge-based approach for interpreting genome-wide expression profiles. *Proceedings of the National Academy of Sciences of the United States of America* **102**, 15545-15550, doi:10.1073/pnas.0506580102 (2005).

48 Mootha, V. K. *et al.* PGC-1alpha-responsive genes involved in oxidative phosphorylation are coordinately downregulated in human diabetes. *Nature genetics* **34**, 267-273, doi:10.1038/ng1180 (2003).

49 Liberzon, A. *et al.* The Molecular Signatures Database (MSigDB) hallmark gene set collection. *Cell systems* **1**, 417-425, doi:10.1016/j.cels.2015.12.004 (2015).

50 Liberzon, A. *et al.* Molecular signatures database (MSigDB) 3.0. *Bioinformatics* **27**, 1739-1740, doi:10.1093/bioinformatics/btr260 (2011).

51 Ashburner, M. *et al.* Gene ontology: tool for the unification of biology. The Gene Ontology Consortium. *Nature genetics* **25**, 25-29, doi:10.1038/75556 (2000).

52 Caru, M. *et al.* Ethical consideration and feasibility demonstration of high-intensity interval training without the use of electrical shocks in mice with and without doxorubicin exposition. *American journal of cancer research* **9**, 2813-2820 (2019).
53 Baruch, D. E., Swain, R. A. & Helmstetter, F. J. Effects of exercise on Pavlovian fear conditioning. *Behavioral neuroscience* **118**, 1123-1127, doi:10.1037/0735-7044.118.5.1123 (2004).
54 Manzanares, G., Brito-da-Silva, G. & Gandra, P. G. Voluntary wheel running: patterns and physiological effects in mice. *Brazilian journal of medical and biological research = Revista brasileira de pesquisas medicas e biologicas* **52**, e7830, doi:10.1590/1414-431X20187830 (2018).
55 Hoppeler, H. Molecular networks in skeletal muscle plasticity. *The Journal of experimental biology* **219**, 205-213, doi:10.1242/jeb.128207 (2016).
56 Dyar, K. A. *et al.* The calcineurin-NFAT pathway controls activity-dependent circadian gene expression in slow skeletal muscle. *Molecular metabolism* **4**, 823-833, doi:10.1016/j.molmet.2015.09.004 (2015).
57 Koike, N. *et al.* Transcriptional architecture and chromatin landscape of the core circadian clock in mammals. *Science* **338**, 349-354, doi:10.1126/science.1226339 (2012).
58 Goodpaster, B. H., He, J., Watkins, S. & Kelley, D. E. Skeletal muscle lipid content and insulin resistance: evidence for a paradox in endurance-trained athletes. *The Journal of clinical endocrinology and metabolism* **86**, 5755-5761, doi:10.1210/jcem.86.12.8075 (2001).
59 Summermatter, S., Baum, O., Santos, G., Hoppeler, H. & Handschin, C. Peroxisome proliferator-activated receptor {gamma} coactivator 1{alpha} (PGC-1{alpha}) promotes skeletal muscle lipid refueling in vivo by activating de novo lipogenesis and the pentose phosphate pathway. *The Journal of biological chemistry* **285**, 32793-32800, doi:10.1074/jbc.M110.145995 (2010).
60 Blair, S. N. *et al.* Physical fitness and all-cause mortality. A prospective study of healthy men and women. *Jama* **262**, 2395-2401, doi:10.1001/jama.262.17.2395 (1989).
61 Lamia, K. A. *et al.* Cryptochromes mediate rhythmic repression of the glucocorticoid receptor. *Nature* **480**, 552-556, doi:nature10700 [pii] 10.1038/nature10700 (2011).
62 Gluchowski, N. L. *et al.* Hepatocyte Deletion of Triglyceride-Synthesis Enzyme Acyl CoA: Diacylglycerol Acyltransferase 2 Reduces Steatosis Without Increasing Inflammation or Fibrosis in Mice. *Hepatology* **70**, 1972-1985, doi:10.1002/hep.30765 (2019).
63 Dobin, A. *et al.* STAR: ultrafast universal RNA-seq aligner. *Bioinformatics* **29**, 15-21, doi:10.1093/bioinformatics/bts635 (2013).
64 Trapnell, C. *et al.* Differential analysis of gene regulation at transcript resolution with RNA-seq. *Nature biotechnology* **31**, 46-53, doi:10.1038/nbt.2450 (2013).
65 Roberts, A., Trapnell, C., Donaghey, J., Rinn, J. L. & Pachter, L. Improving RNA-Seq expression estimates by correcting for fragment bias. *Genome biology* **12**, R22, doi:10.1186/gb-2011-12-3-r22 (2011).

66 Trapnell, C. *et al.* Differential gene and transcript expression analysis of RNA-seq experiments with TopHat and Cufflinks. *Nature protocols* **7**, 562-578, doi:10.1038/nprot.2012.016 (2012).
67 Love, M. I., Huber, W. & Anders, S. Moderated estimation of fold change and dispersion for RNA-seq data with DESeq2. *Genome biology* **15**, 550, doi:10.1186/s13059-014-0550-8 (2014).
68 Reich, M. *et al.* GenePattern 2.0. *Nature genetics* **38**, 500-501, doi:10.1038/ng0506-500 (2006).
69 Wallace, M. *et al.* Enzyme promiscuity drives branched-chain fatty acid synthesis in adipose tissues. *Nature chemical biology* **14**, 1021-1031, doi:10.1038/s41589-018-0132-2 (2018).

FIGURE TITLES AND LEGENDS

Figure 1: Time of day impacts maximum speed in trained but not sedentary mice. (A) Schematic diagram of the experimental setup. c57BL/6J mice were weaned at 4 weeks of age into cages without running wheels. When they were 9 weeks old, their maximum sprint speed was determined using a motorized treadmill at either zeitgeber time (ZT, hours after lights on) 13 or 21. Then, they were transferred to cages with running wheels for six weeks, and their maximum sprint speed was determined at either ZT13 or ZT21 again. (B) Maximum speeds achieved by male mice described in (A). Each symbol represents a unique sedentary (black) or trained (red) animal. ** $P < 0.01$, **** $P < 0.00001$ by two-way ANOVA followed by Tukey's multiple comparison test. (C) Diagram of manual and electrical aversive stimuli used to motivate continued treadmill running. (D) Maximum speeds achieved at ZT13 by c57BL/6J male mice using manual (black) or electrical (yellow) stimuli shown in (C). (E) Temporal profile of running wheel activity during the training period, in one-hour bins. For each ZT, the total activity recorded in the preceding hour is shown. (F) Expression of the indicated transcripts measured by qPCR in RNA isolated from quadriceps of sedentary (black) or trained (red) male c57BL/6J mice collected at the indicated ZTs. Data represent the mean ± s.e.m. for 6 samples per condition each measured in triplicate. ** $P < 0.01$, *** $P < 0.001$, **** $P < 0.0001$ for a main effect of training (red) or of ZT (black) by two-way ANOVA.

Figure 2: Training remodels the skeletal muscle circadian transcriptome. (A) Schematic diagram of the experimental setup. C57BL/6J mice were weaned at 4 weeks of age into cages without running wheels. When they were 9 weeks old, they were transferred to individually housed cages without (SED) or with (RW) running wheels for six weeks. On the first day of week 7 (when they were 15 weeks old), muscles were collected every four hours starting at ZT1. (B) Principal component analysis reveals natural clustering of transcriptional phenotypes by ZT in both SED and RW datasets. (C) Heat maps representing expression levels (red high, blue low) of transcripts revealed by CircWave to be expressed with a circadian rhythm in plantaris muscles from sedentary (SED, left), running wheel trained (RW, right) or both (center). Each horizontal line represents a single transcript. Transcripts are ordered by peak phase. (D)

Venn diagram showing the overlap of specific transcripts determined to be rhythmic in each training state. (E) Average detection of the indicated transcripts in sequenced RNA from sedentary (SED, black) or trained (RW, red) mice. (F) Detection of CRY1 and CRY2 by immunoblot in protein lysates prepared from plantaris muscles collected at the indicated ZTs. Each lane represents a unique plantaris sample. The rightmost lanes contain nuclear extracts from quadriceps muscles of wildtype and *Cry1*$^{-/-}$;*Cry2*$^{-/-}$ mice used as a control for antibody specificity. Data are a representative example of three sets of lysates from unique animals. (G) Quanitation of the data shown in (F) in which the signal for each sample was normalized to the average of all detected signals on the same Western blot exposure. Data represent the mean + s.d. for three experiments. *** $P < 0.001$ for a main effect of training state by two-way ANOVA.

Figure 3: Metabolic and structural elements response to training. (A) Heat map representing expression levels (red high, blue low) of the 100 transcripts revealed by DESeq2 to exhibit the greatest increase (top) or decrease (bottom) in transcription in response to training. Each horizontal line represents a single transcript. Individual gene names for select transcripts are indicated on the right. (B-D) Average detection of the indicated transcripts in sequenced RNA from sedentary (SED, black) or trained (RW, red) mice. (E) Detection of DGAT2 and CRYAB by immunoblot in protein lysates prepared from plantaris muscles collected at the indicated ZTs. Each lane represents a unique plantaris sample. Data are a representative example of two sets of lysates from unique animals. (F) Quantitation of the data shown in (E) in which the signal for each sample was normalized to the average of all detected signals on the same Western blot exposure. Each symbol represents a unique sample. ** $P < 0.01$ for a main effect of training state by two-way ANOVA.

Figure 4: Training alters glycogen in a time of day dependent manner. (A) Heat map representing expression levels (red high, blue low) of transcripts involved in glycogen metabolism that are included in the “Glycogen Metabolism” Hallmark gene set defined by MSigDB. Each horizontal line represents a single transcript. Individual gene names for select transcripts are indicated on the right. (B) Schematic diagram showing the function of selected enzymes in glycogen metabolism. (C, D) Average detection of the indicated transcripts in sequenced RNA from sedentary (SED, black) or trained (RW, red) mice. (E) Detection of phosphorylated and total GSK3α and GSK3β, HK2, and SDHA by immunoblot in protein lysates prepared from plantaris muscles collected at the indicated ZTs. Each lane represents a unique plantaris sample. (F, G) Quantitation of the data shown in (E) ** $P < 0.01$ by t-test. (H, I, K, L) Glycogen content measured in quadriceps (H, I) or liver (K, L) from sedentary (black) or trained (red) mice not subjected to sprint testing (H, K), or trained mice immediately after sprint testing (I, L) at the indicated ZTs. *** $P < 0.001$ by two-way ANOVA with post-hoc analysis. (J,M) Correlation between maximum sprint speed achieved and glycogen remaining in the quadriceps (J) or liver (L) immediately after the sprint test performed at ZT21.

Figure 5: Training alters carbohydrate and lipid utilization in a time of day dependent manner. (A, B) Heat maps representing expression levels (red high, blue low) of transcripts included in the “Oxidative Phosphorylation” Hallmark gene set (A) or

the “GO_SODIUM_SOLUTE_TRANSPORTER_ACTIVITY” gene set (B) in MSigDB. Each horizontal line represents a single transcript. (B, F) Average detection of *Slc6a8* and *Slc20a1* (B) or *Elovl1* and *Elovl2* (F) in plantaris muscle RNA sequencing. (D, E) Total content of all (D) or individual (E) triacylglyceride species measured by quantitative mass spectrometry in extracts from quadriceps muscles collected from sedentary (SED) or trained (RW) male mice at the indicated ZTs. Data represent the mean ± s.e.m. of six samples per condition. * $P < 0.05$ vs ZT13, # $P < 0.05$ vs SED by two-way ANOVA. (G-K) Measurement of the indicated metabolites in blood collected before (black) or immediately after (red) sprint to exhaustion. NEFA, non-esterified fatty acids. In (G-K) * $P < 0.05$, ** $P < 0.01$, **** $P < 0.0001$ by ANOVA.

Methods

Mouse Models

C57BL/6J mice were purchased from the Scripps Research breeding colony at six weeks of age. They were maintained in standard 12:12 light:dark conditions unless otherwise indicated and were group housed except when given voluntary access to running wheels, in which case they were singly housed in running wheel cages. They were given ad libitum access to normal mouse chow and water. All animal care and treatments were approved and overseen by The Scripps Research Institutional Animal Care and Use Committee under protocol #10-0019.

Treadmill Exercise Testing

Treadmill running performance was assessed at ZT6, ZT13, ZT16 or ZT21 in 5-12 mice per group. Untrained, sedentary male mice were tested at 9 weeks of age, and then underwent six weeks of voluntary running wheel training and were tested again after training at 15 or 17 weeks of age. A separate group of male mice were maintained in a sedentary state and tested at 9 and 17 weeks of age. Running performance was also assessed in age-matched female mice following 6 weeks of voluntary running wheel-training when they were 15 weeks old. In each case, mice were habituated to a motorized treadmill (Exer3/6M with 10grade, Columbus Instruments) in the week prior to experimentation with three 10 min sessions of walking/running at a slow speed (first session up to 10 m/min; second session up to 12.5 m/min; third session up to 15 m/min). On the day of experimentation to assess sprint capacity, the treadmill was started at a speed of 6 m/min for a period of 3 min. Subsequently, the speed was continuously increased every minute by 1 m/min, until the mouse could no longer sustain that current sprint speed. For the majority of experiments, the shocker grid at the end of the treadmill was turned off and mice were encouraged to continue running by manually pushing them back onto the treadmill from the platform. They were considered unable to sustain the speed when they remained on the platform or repeatedly fell onto the platform five or more times within one minute. For experiments investigating the influence of electrical stimulation on outcomes, the shocker grid was set to 0.15 mA intensity and 1 Hz frequency. Blood glucose (Aviva Accu-chek, Roche Diagnostics), lactate (Lactate Scout, SensLab) and ketone (Precision Xtra, Abbott Laboratories) levels were assessed via the tail vein at baseline (week prior to experimentation) and immediately post-sprint run.

Running Wheel Training

9-week-old male or female mice were single housed and given access to running wheels for 6 weeks in standard 12:12 light:dark conditions with ad libitum access to food and water. Voluntary running wheel activity was analyzed with ClockLab (Actimetrics) using digital recordings of wheel rotations taken over at least a 2 week period.

Western Blots

Protein lysates (30-50 µg) prepared from quadriceps or plantaris muscles were separated by SDS-PAGE and transferred to polyvinylidine difluoride (PVDF) membranes. For mitochondrial blots, mitochondria were isolated by subcellular

fractionation, as described previously (Dimauro et al.). Proteins were detected by standard Western blotting procedures. Antibodies used to detect HK2, GSK3a/b, and phosphor-GSK3a/b were from Cell Signaling Technology (catalog numbers C64G5, 9331, 5676). Commercially available antibodies were used to detect SDHA (Life Technologies #459200), CRYAB (Enzo Life Sciences, ADI-SPA-222-D), and Tubulin (Sigma, T5168). CRY1 and CRY2 were detected using antibodies that we have previously described [61]. DGAT2 was detected using an antibody that has been previously described [62]. Imaging and band quantification were carried out using a ChemiDoc Imaging System (Bio-Rad).

RNA extraction and quantitative PCR

RNA was extracted from quadriceps or plantaris muscle tissue (collected at specified ZTs) by homogenization in QIAzol (Qiagen) lysis reagent. Phase separation was achieved with chloroform and RNA was precipitated with a standard isopropanol/ethanol procedure. Pelleted and washed RNA was resuspended in RNase-free water and then quantified with a NanoDrop system (Thermo Fisher). cDNA was prepared from 1 µg RNA by reverse transcription with iScript supermix (BioRad). Quantitative real-time PCR was carried out with SYBR Green (BioRad) and a CFX96 Real-Time PCR System (BioRad). Gene quantification was normalized to *Hprt.* (Table of sequencing primers below).

Gene	Forward Primer (5'-3')	Reverse Primer (5'-3')
Cry1	GCT ATG CTC CTG GAG AGA ACG T	TGT CCC CGT GAG CAT AGT GTA A
Cry2	CTG GCG AGA AGG TAG AGT GG	GAC GCA GAA TTA GCC TTT GC
Cpt1	GCA CAC CAG GCA GTA GCT TT	CAG GAG TTG ATT CCA GAC AGG TA
Egln1	TAC AGG ATA AAC GGC CGA AC	CAT GTC ACG CAT CTT CCA TC
Egln2	CTG TCT GGT ATT TTG ATG CCA AGG	CGG CTG TGA TAC AGG TAC TTG G
Egln3	ACG TGG AGC CCA TTT TTG AC	TTG GCT TCT GCC CTT TCT TC
Hif1a	ACA AGT CAC CAC AGG ACA G	AGG GAG AAA ATC AAG TCG
Hk2	GAA GGG GCT AGG AGC TAC CA	CTC GGA GCA CAC GGA AGT T
Hprt	TGC TCG AGA TGT CAT GAA GG	TAT GTC CCC CGT TGA CTG AT
Il6	CAT AGC TAC CTG GAG TAC ATG AAG	GGA AAT TGG GGT AGG AAG GAC TA
Ldha	GGG CTA CAA GCA TCT TGA GAG	GAC ACG TTG CAC CTG ACT G
Ldhb	AGT CTC CCG TGC ATC CTC AA	AGG GTG TCC GCA CTC TTC CT
Slc16a1	TGT TAG TCG GAG CCT TCA TTT C	CAC TGG TCG TTG CAC TGA ATA
Slc16a7	GCT GGG TCG TAG TCT GTG C	ATC CAA GCG ATC TGA CTG GAG

Slc16a3	TCA CGG GTT TCT CCT ACG C	GCC AAA GCG GTT CAC ACA C
Pdk4	AGG GAG GTC GAG CTG TTC TC	GGA GTG TTC ACT AAG CGG TCA
Per2	TGT GCG ATG ATG ATT CGT GA	GGT GAA GGT ACG TTT GGT TTG
Ppargc1a	AAC CAG TAC AAC AAT GAG CCT G	AAT GAG GGC AAT CCG TCT TCA
Prkaa1	AGA AGC AGA AGC ACG ACG	TCA AGG CTC CGA ATC TTC TGC C
Prkab2	GGC AAG GAG GTC TTC ATC TCT	AGG ATG GCA ACG AAG TCA TTA TG
Ucp3	CTG CAC CGC CAG ATG AGT TT	ATC ATG GCT TGA AAT CGG ACC
Vegfa	CTT GTT CAG AGC GGA GAA AGC	ACA TCT GCA AGT ACG TTC GTT

RNA-seq library preparation, sequencing, and analysis

Total mouse plantaris RNA was isolated using Trizol (Invitrogen) and the RNeasy mini kit with on-column DNase digestion (Qiagen). RNA purity was assessed by Agilent 2100 Bioanalyzer. Sequencing libraries were prepared from 100 ng of total RNA using the TruSeq Stranded Total RNA sample preparation kit (Illumina) according to the manufacturer's protocol. Briefly, mRNA was purified, fragmented and used for first- and second-strand cDNA synthesis followed by adenylation of 3′ ends. Samples were ligated to unique adaptors and subjected to PCR amplification. Libraries were then validated using the 2100 BioAnalyzer (Agilent), normalized and pooled for sequencing. RNA-Seq libraries prepared from three biological replicates for each experimental timepoint were subjected to single-ended sequencing on the Illumina HiSeq 2500 using barcoded multiplexing and a 90-bp read length. Image analysis and base calling were done with Illumina CASAVA-1.8.2. Short read sequences were mapped to a UCSC mm10 reference sequence using the RNA-seq aligner STAR v2.7.2b [63]. Known splice junctions from mm10 were supplied to the aligner and de novo junction discovery was also permitted. Differential gene expression analysis, statistical testing and annotation were performed using Cuffdiff v2.2.1 [64]. Transcript expression was calculated as gene-level relative abundance in fragments per kilobase of exon model per million mapped fragments (FPKM) and employed correction for transcript abundance bias [65]. Data visualization, quality control and principal component analysis were performed in R using the CummeRbund package [66]. CircWaveBatch v5.0 (Hut, R., www.euclock.org/results/item/*circ-wave-batch*.html) was used to determine circadian rhythmicity of individual genes within the RNA-seq dataset. Prior to analysis, low expression genes were culled if the sum of FPKM values across all replicates and both treatments, 34 samples in all, was < 20. This left 10,778 genes for further evaluation.

To identify genes with differential expression between training states including all Zeitgeber Times as a confounding factor, we employed the DESeq2 module [67] in GenePattern [68]. To identify sets of genes coordinately altered by training state, we used the GSEA module [47]. To identify sets of genes in which circadian patterns of expression

were coordinately altered by training state, we used GSEA pre-ranked using a list of genes ranked by the pANOVA output from CircWave. All GSEA runs first queried the c1.all.v7 (Hallmarks) gene set database and then c2.all.v7 (curated) in MSigDB [49,50]. Prior to these analyses, low expression genes were culled if the FPKM value was < 5 in 25 or more samples across all replicates and both treatments.
RNA-Seq data reported in this paper have been deposited in the National Center for Biotechnology Information (NCBI) Sequence Read Archive (SRA) database, BioProject ID PRJNA639978.

Tissue glycogen analysis
Quadriceps and liver glycogen content was assessed from tissues dissected under basal conditions or immediately post-sprint exercise testing. Glycogen was detected using a commercial glycogen assay kit (Sigma, MAK016), as per manufacturer's instructions. Tissue (~50-100 mg) was homogenized in MQ water and glycogen concentration determined by a coupled enzymatic assay. The colorimetric reaction was detected at 570 nm in a microplate reader (VersaMax).

Serum triglyceride analysis
Circulating triglycerides were assessed immediately post-sprint exercise testing. Blood was collected by cardiac puncture and left undisturbed at room temperature for 30 min. After centrifugation at 4°C for 10 min at 2000g, the serum supernatant was collected. Triglycerides were detected from serum using a commercially available triglyceride assay kit (Sigma, MAK266). Triglyceride concentration was determined by enzymatic breakdown to glycerol. The colorimetric reaction from glycerol oxidation was detected at 570 nm in a microplate reader (VersaMax).

Serum NEFA analysis
Circulating non-esterified fatty acids (NEFAs) were assessed immediately post-sprint exercise testing. Serum was isolated as described above. NEFAs were detected from serum using a commercially available NEFA assay reagents (Wako Diagnostics, 999-34691). NEFA concentration was determined by the enzymatic acylation of coenzyme A; the colorimetric reaction from Acyl-coA oxidation was detected at 550 nm in a microplate reader (VersaMax).

Tissue polar metabolite extraction
Frozen tissue samples (20-30 mg) were homogenized for 2 min using ceramic beads (Precellys 2 mL Hard Tissue Homogenizing Ceramic Beads Kit, Bertin Instruments, US) in 500 µL -20 °C methanol, ice-cold 400µL saline and ice-cold dH_2O containing amino acid isotope labelled internal standards (Cambridge Isotope Laboratories, #MSK-A2-1.2). An aliquot of homogenate (50µL) was dried under air and resuspended in RIPA buffer for protein quantification using BCA assay (BCA Protein Assay, Lambda, Biotech Inc., US). To the remaining homogenate, 1 mL of chloroform was added and the samples were vortexed for 5 min followed by centrifugation at 4°C for 5 min @ 15 000g. The organic phase was collected and the remaining polar phase was re-extracted with 1 mL of chloroform. An aliquot of the polar phase was collect and vacuum-dried at 4°C and subsequently derivatized with 2% (w/v) methoxyamine hydrochloride (Thermo

Scientific) in pyridine for 60 min following by 30 min sialyation N-tertbutyldimethylsilyl-N-methyltrifluoroacetamide (MTBSTFA) with 1% tert-butyldimethylchlorosilane (tBDMS) (Regis Technologies) at 37°C. Polar derivatives were analyzed by GC-MS using a DB-35MS column (30m x 0.25mm i.d. x 0.25 µm, Agilent J&W Scientific) installed in an Agilent 7890A gas chromatograph(GC) interfaced with an Agilent 5975C mass spectrometer (MS) as previously described [69].

Tissue triglyceride extraction

Frozen tissue samples (20-30 mg) were homogenized for 2 min using ceramic beads (Precellys 2 mL Hard Tissue Homogenizing Ceramic Beads Kit, Bertin Instruments, US) in 500 µL -20 °C methanol, ice-cold 400µL saline and ice-cold dH_2O containing C12 MAG (1-0-dodecyl-rac-glycerol, #SC-201977, Santa Cruz) as internal standard. To the remaining homogenate, 1 mL of chloroform was added and the samples were vortexed for 5 min followed by centrifugation at 4°C for 5 min @ 15 000g. The organic phase was collected and 2 µL of formic acid was added to the remaining polar phase, which was re-extracted with 1 mL of chloroform. Combined organic phases were dried under air flow and the pellet was resuspended in 125 µL of chloroform. Triglyceride species were separated chromatographically on a C5 column (Luna, 100 x 2 mm, 5 µm, Phenomenex). Mobile phase A was composed of 95:5 ratio of water:methanol, 0.1 % formic acid and 5 mM ammonium formate, and mobile phase B was 60:35:5 isopropanol:methanol:water, 0.1% formic acid and 5 mM ammonium formate. The chromatography gradient elution was as follows: 0 min, 0% B, flow rate 0.1 ml/min; 5 min, 0% B, flow rate 0.4 ml/min; 50 min, 100% B, flow rate 0.4 ml/min; 50.1 min, 100% B, flow rate 0.5 ml/min, 67 min; 100% B, flow rate 0.5 ml/min; 67.5 min, 0% B, flow rate 0.5 ml/min and 76 min, 0% B, flow rate 0.5 ml/min. Liquid chromatography mass spectrometry was performed on an Agilent 6460 QQQ LC-MS/MS instrument. Triglyceride species were analyzed by SRM of the transition from precursor to product ions at associated optimized collision energies and fragmentor voltage (Table below).

Triglyceride species	Parent Ion	Daughter Ion	CE
C12 Mag	261.3	261.3	0
TAG C14:0/C14:0/C14:0	740.7	495.5	40
TAG C14:0/C14:0/C15:0	754.7	495.5	40
TAG C14:0/C16:0/C16:0	796.7	551.5	40
TAG C16:0/C16:0/C16:0	824.7	551.5	40
TAG C16:0/C16:0/C16:1	822.7	551.5	40
TAG C16:0/C16:1/C16:1	820.7	549.5	40
TAG C16:1/C16:1/C16:1	818.7	547.5	40
TAG C16:0/C16:0/C17:0	838.7	551.5	40
TAG C16:0/C16:0/C18:0	852.8	551.5	40
TAG C16:0/C16:0/C18:1	850.8	577.5	40
TAG C16:0/C16:0/C18:2	848.8	575.5	40
TAG C16:0/C16:0/C18:3	846.7	551.5	40
TAG C16:1/C16:1/C18:1	846.7	547.5	40
TAG C16:0/C17:0/C18:0	866.8	593.5	40
TAG C17:0/C17:0/C17:0	866.8	579.5	40

TAG C16:0/C17:0/C18:1	864.8	565.5	40
TAG C16:0/C16:0/C20:0	880.7	551.5	40
TAG C16:0/C18:0/C18:1	878.8	605.5	40
TAG C16:0/C18:0/C18:2	876.8	575.5	40
TAG C16:0/C16:0/C20:4	872.7	551.5	40
TAG C17:0/C18:0/C18:1	892.8	593.5	40
TAG C16:0/C18:0/C20:0	908.8	635.5	40
TAG C16:0/C16:0/C22:6	924.7	651.5	40
TAG C16:0/C17:0/C22:6	910.7	565.5	40
TAG C16:0/C18:0/C22:6	924.7	651.5	40

Statistical analysis

Statistical analyses were performed using GraphPad Prism 8 software. Unless otherwise indicated, ANOVA was used to determine significance with a threshold of 0.05 acceptable false positive ($P < 0.05$).

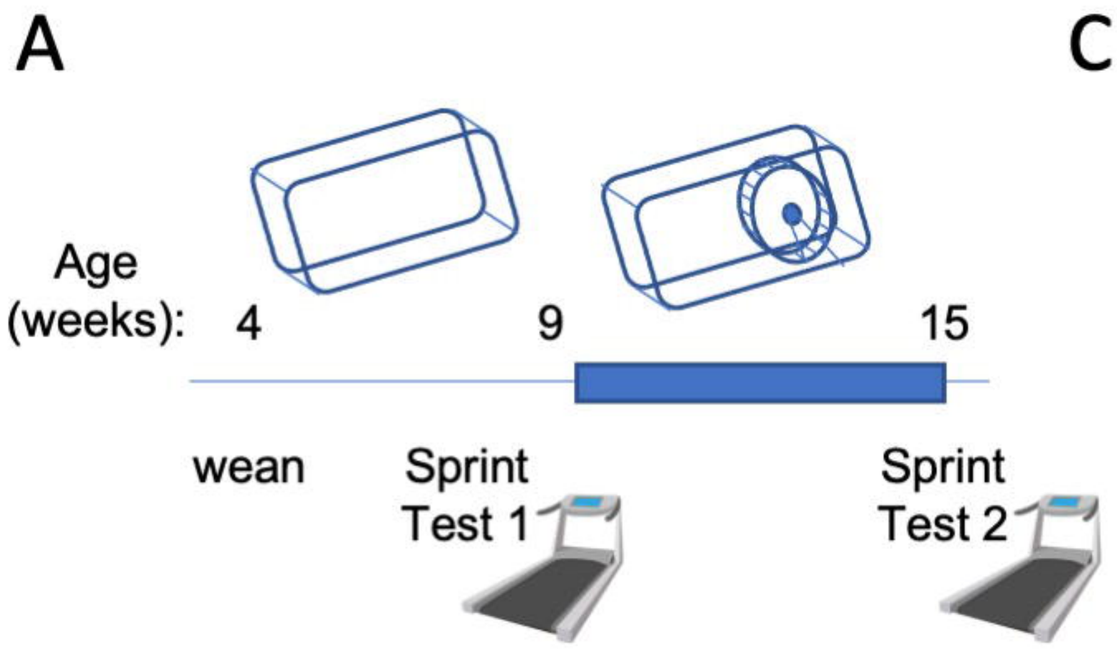

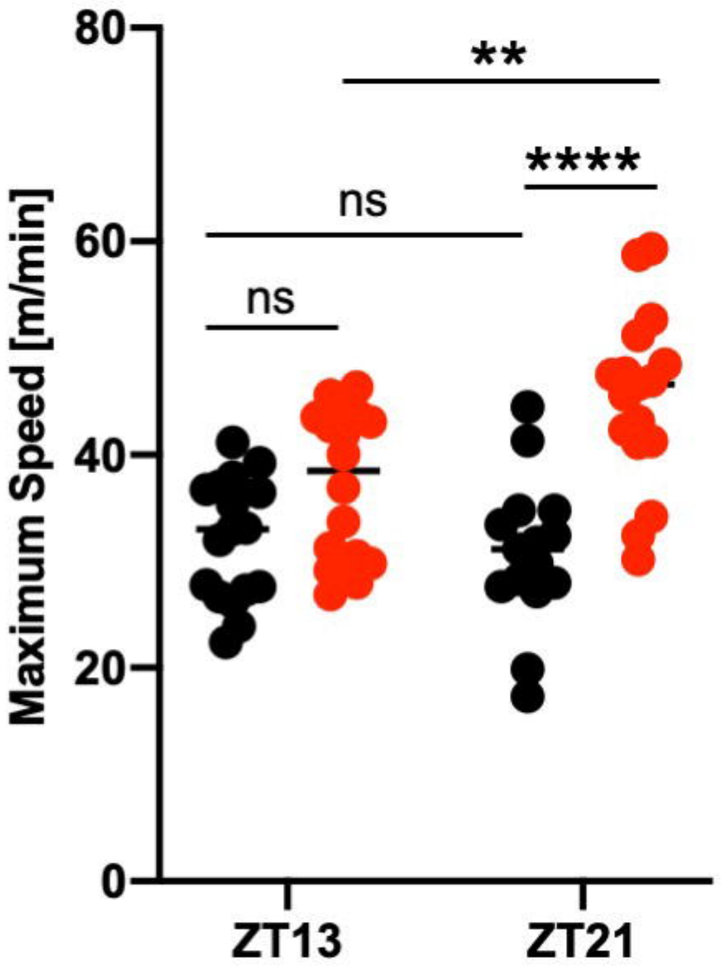

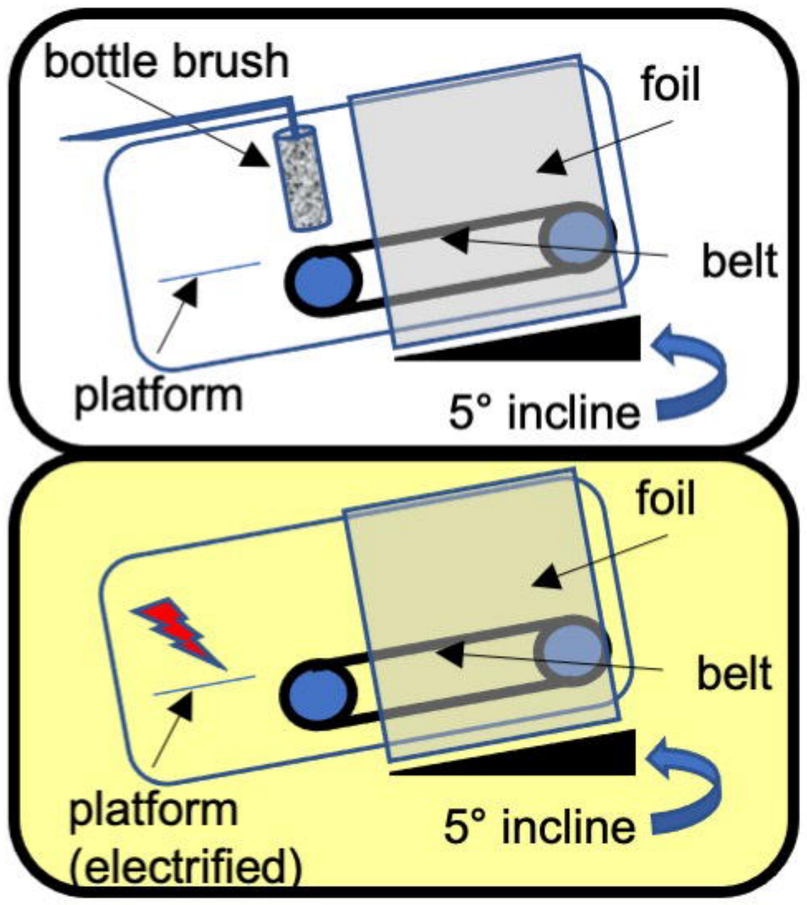

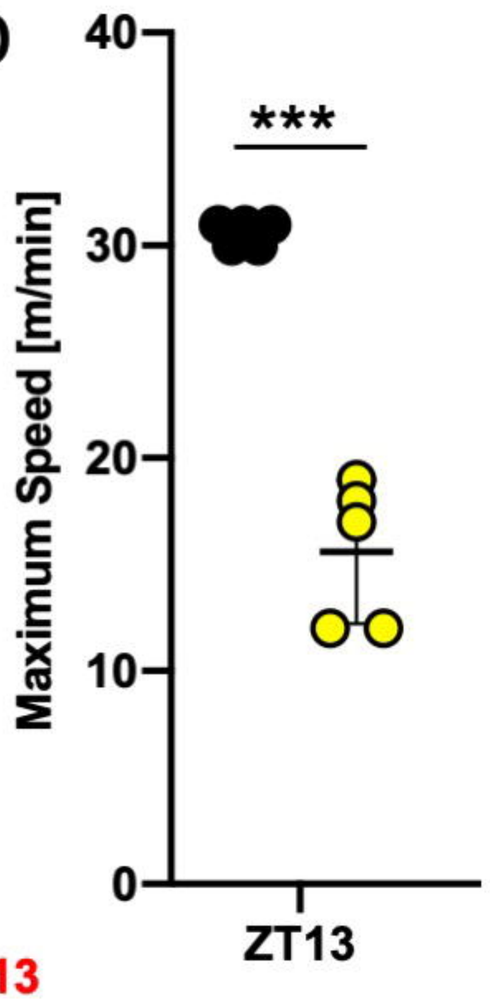

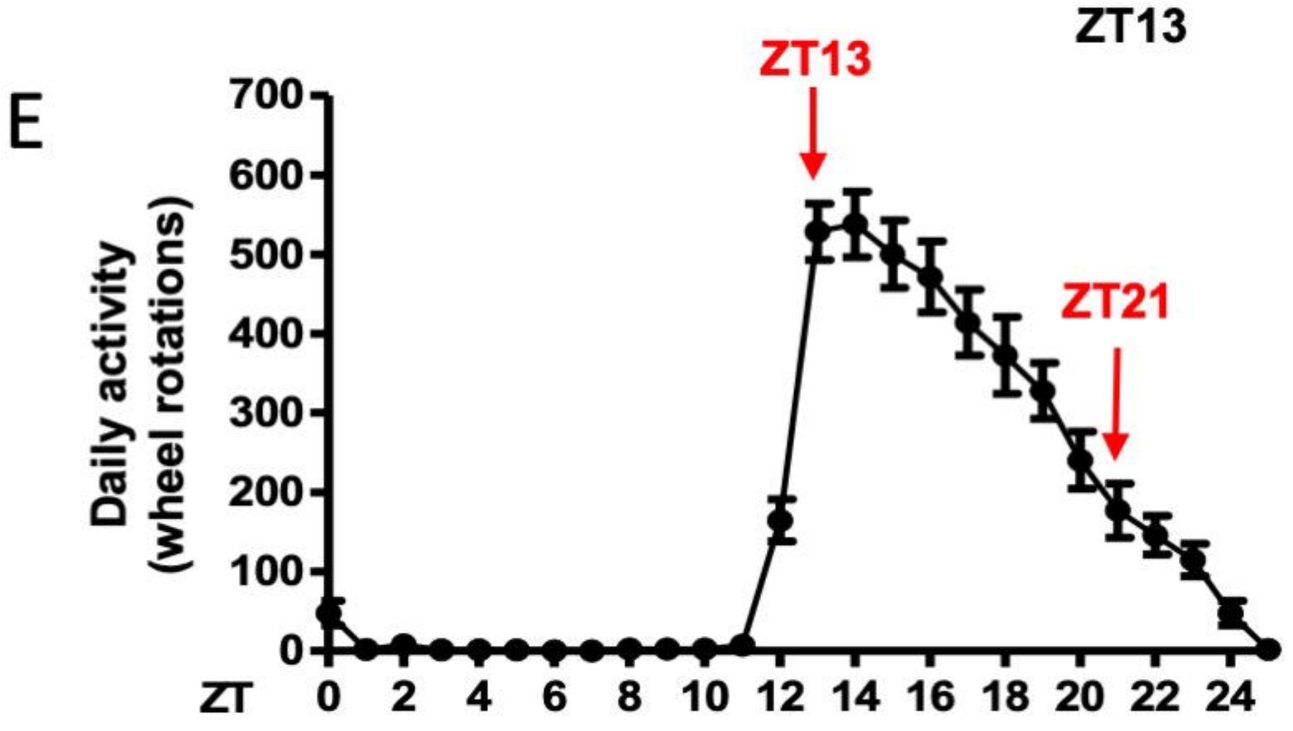

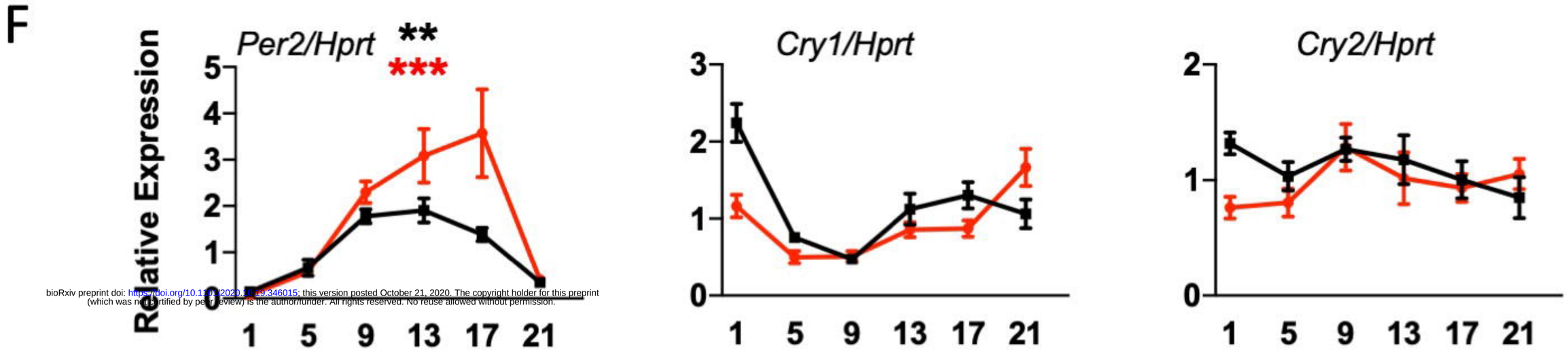

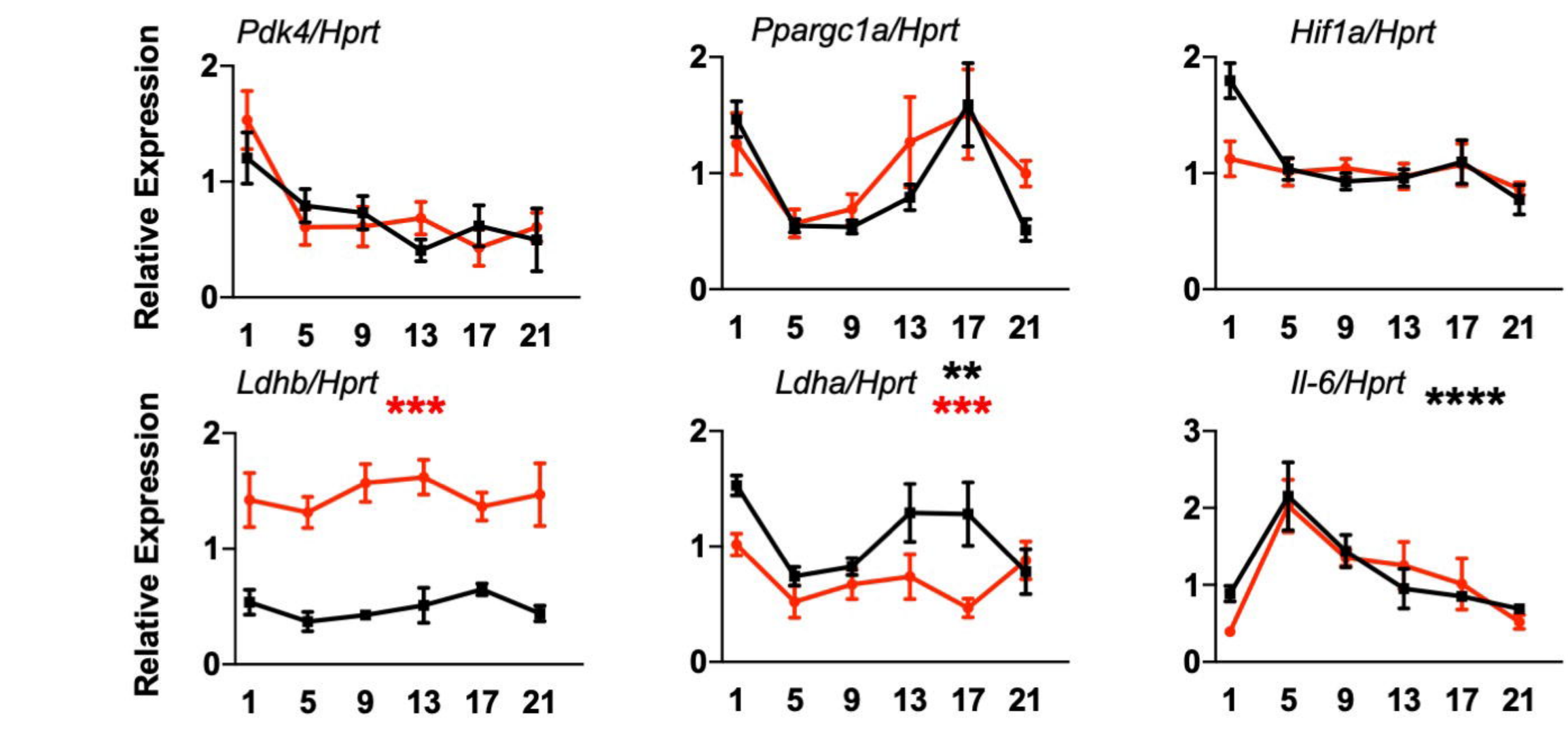

Fig 1

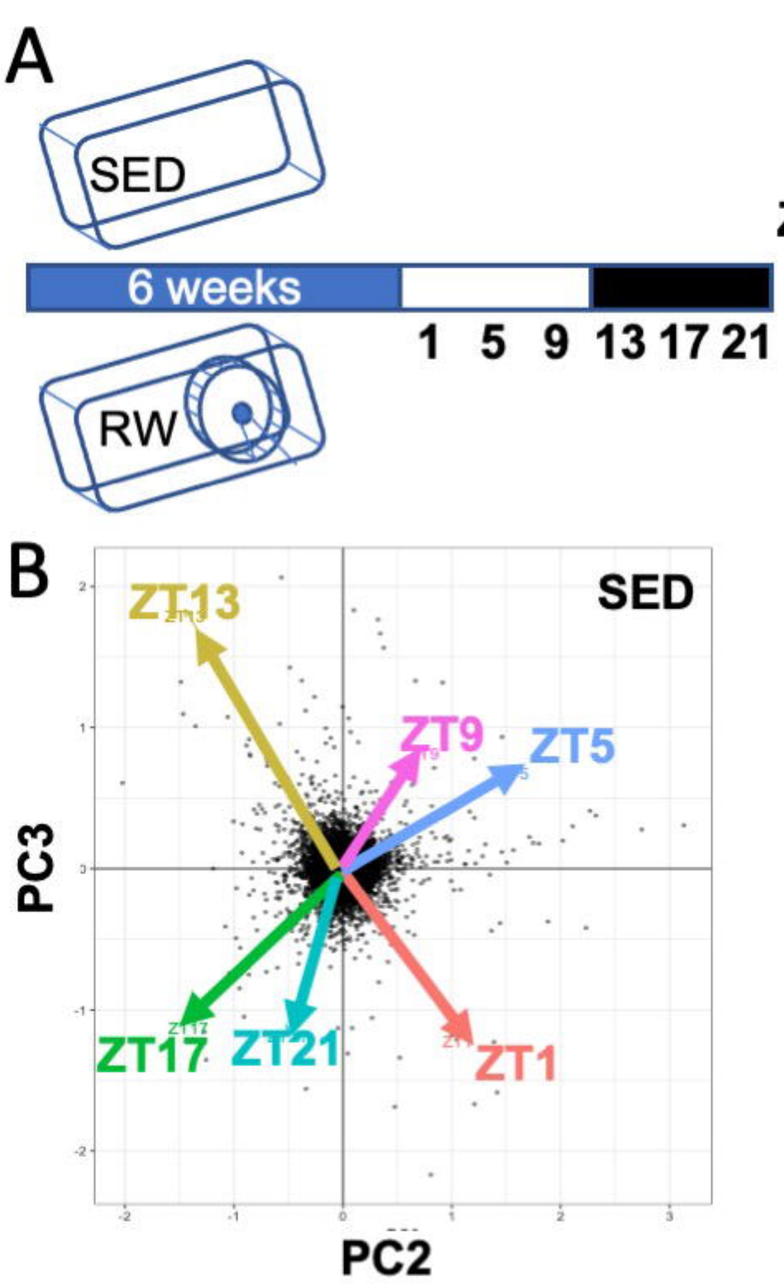

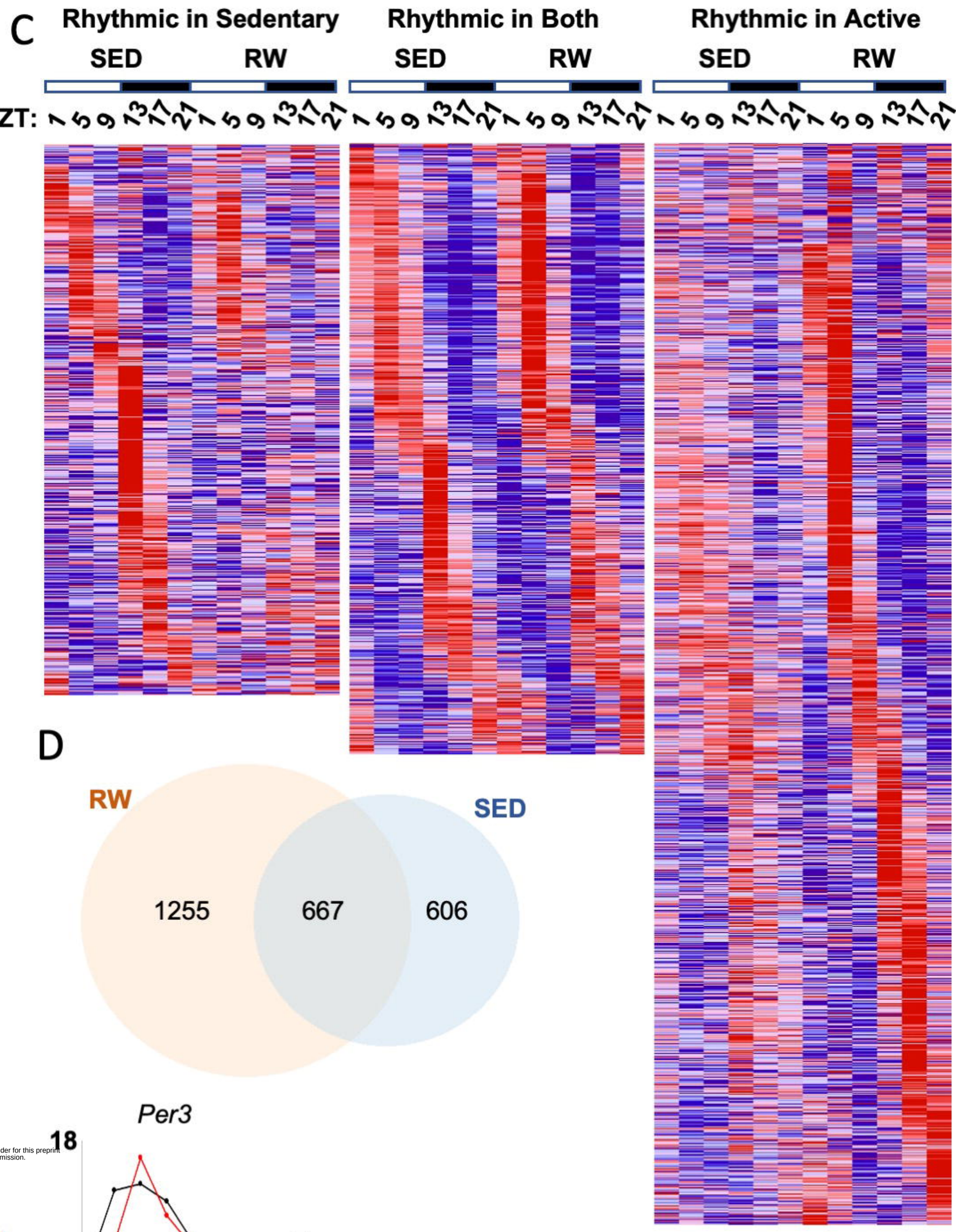

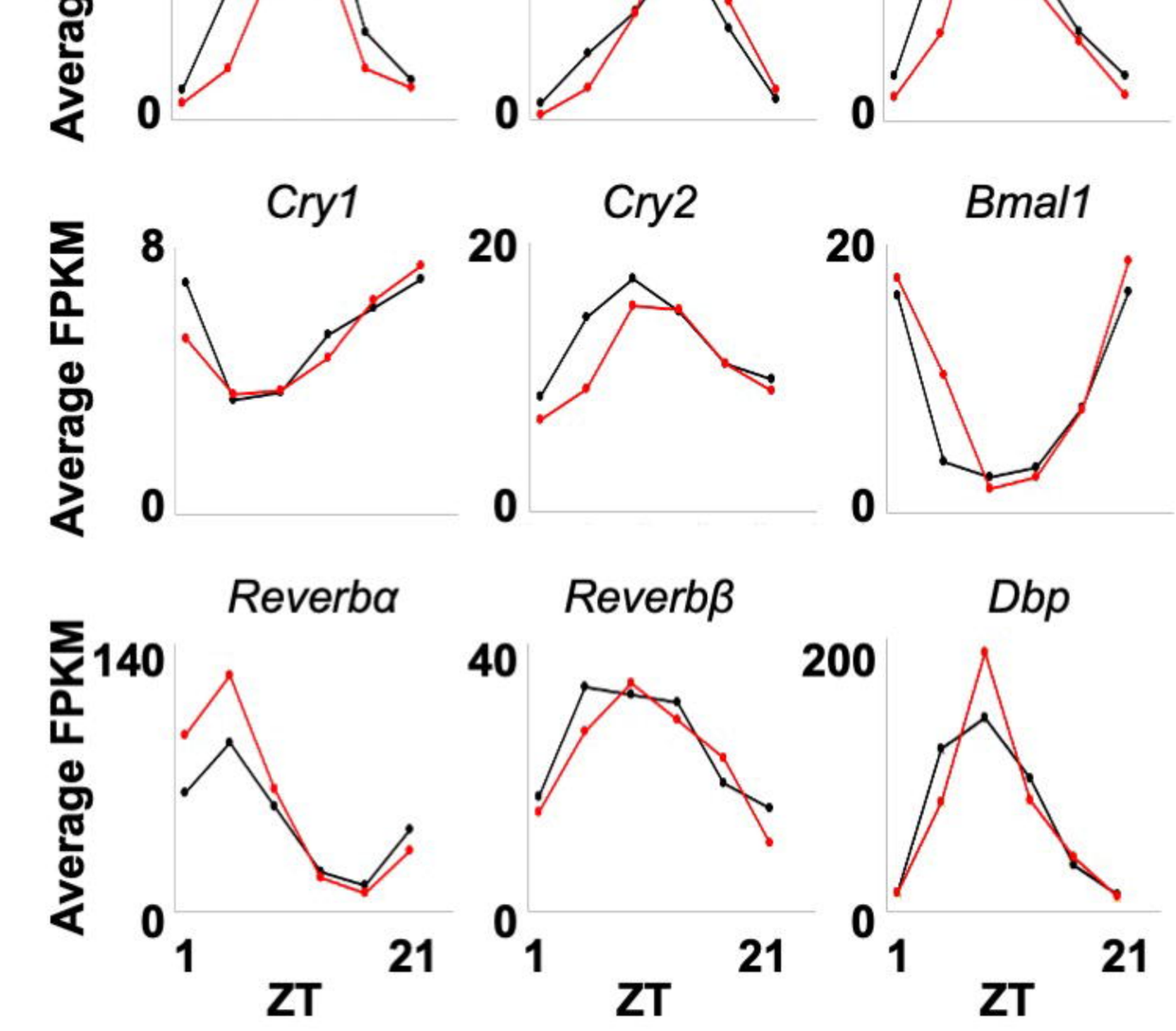

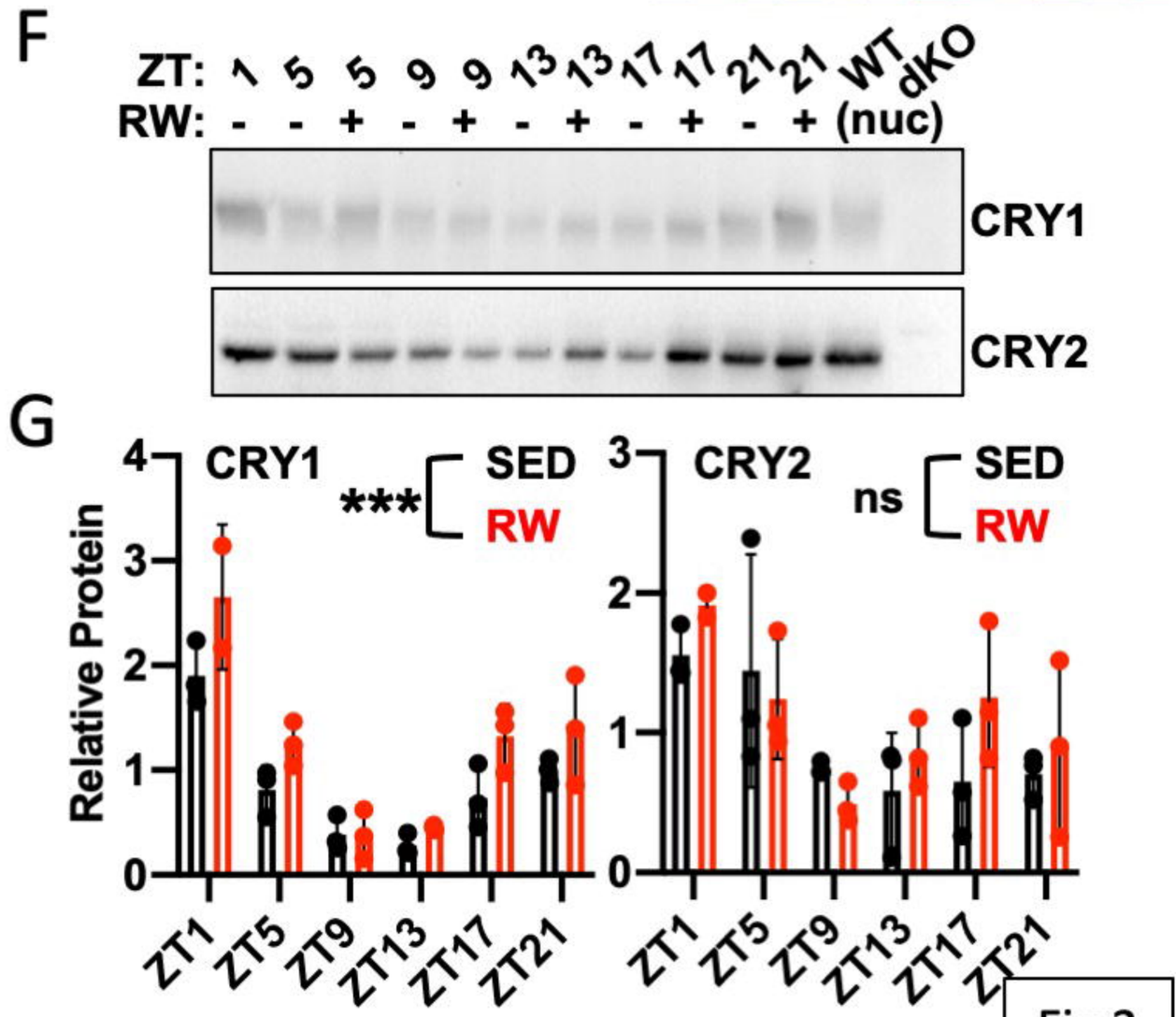

Fig 2

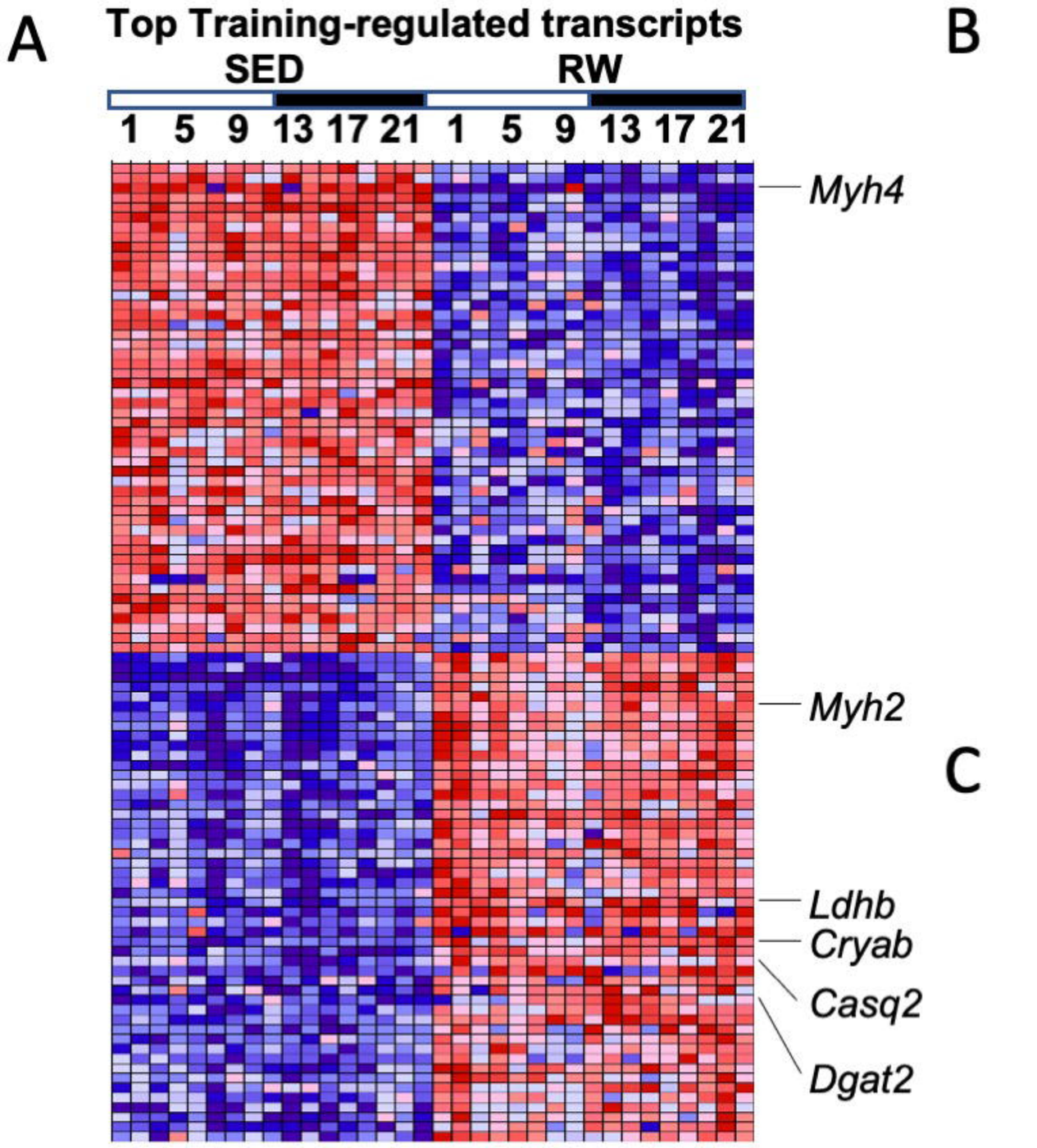

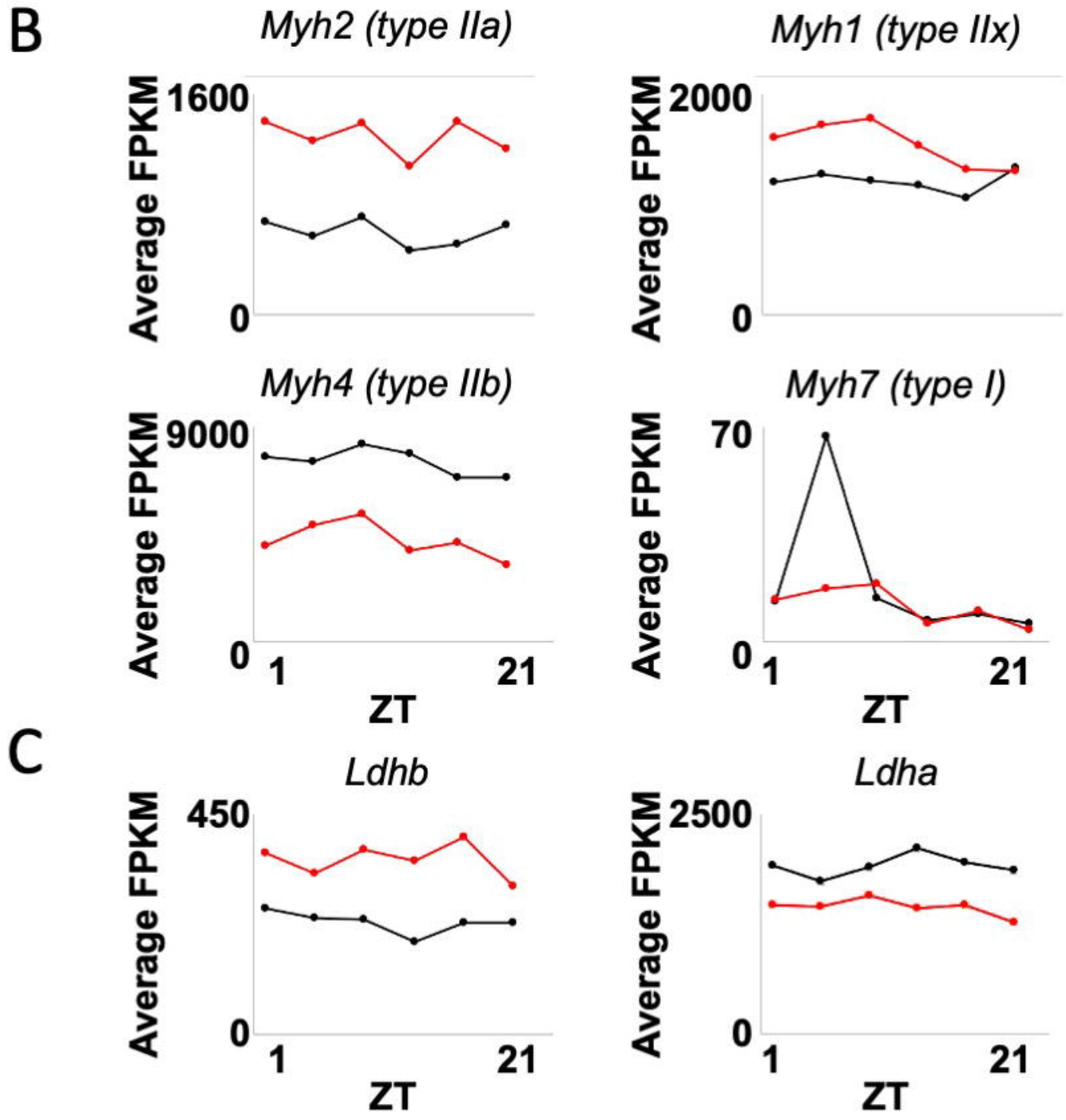

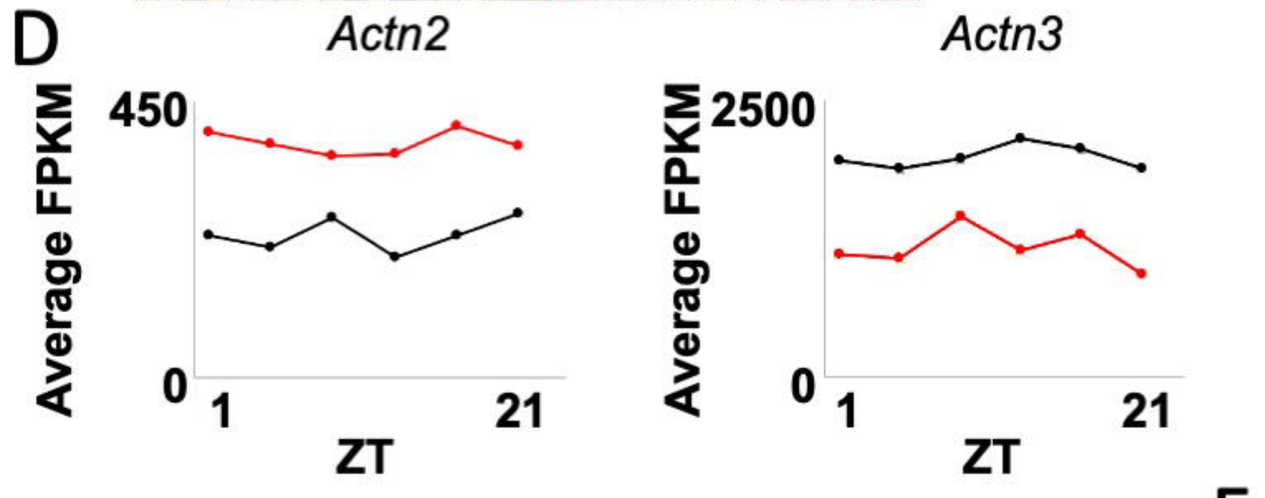

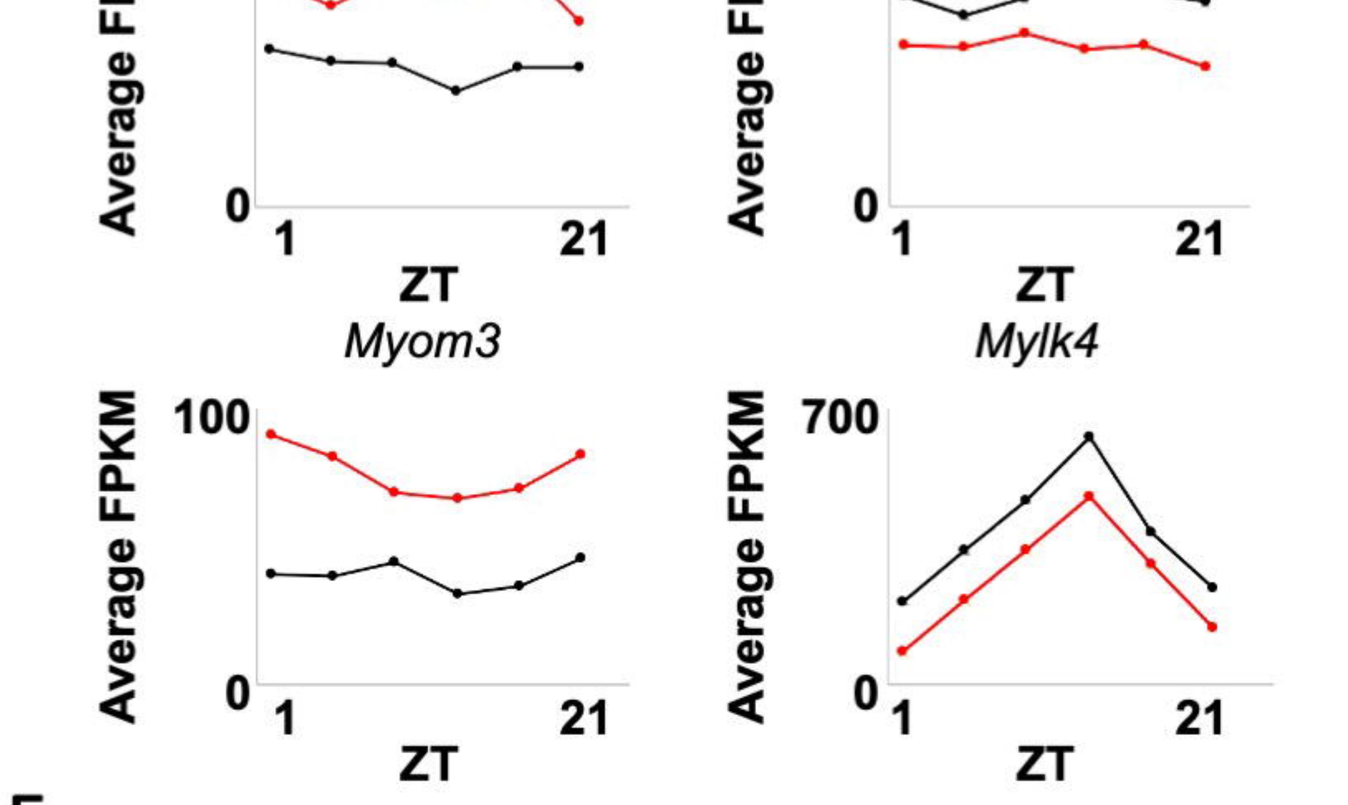

Fig 3

Fig 4

Fig 5